ANALYSIS OF THE NETWORK DYNAMICS OF TRANSFORMING GROWTH FACTOR - β1 BISTABLE ACTIVATION, WITH IMPLICATIONS ON BISTABILITY AND COMBINATION THERAPY

LI HUIPENG

NATIONAL UNIVERSITY OF SINGAPORE

2014

ANALYSIS OF THE NETWORK DYNAMICS OF TRANSFORMING GROWTH FACTOR - β1 BISTABLE ACTIVATION, WITH IMPLICATIONS ON BISTABILITY AND COMBINATION THERAPY

LI HUIPENG

2014

ANALYSIS OF THE NETWORK DYNAMICS OF TRANSFORMING GROWTH FACTOR - β1 BISTABLE ACTIVATION, WITH IMPLICATIONS FOR BISTABILITY AND COMBINATION THERAPY

LI HUIPENG

(B.S. (Physics), Fudan University, Shanghai, China)

A THESIS SUBMITTED

FOR THE DEGREE OF DOCTOR OF PHILOSOPHY

IN COMPUTATIONAL AND SYSTEMS BIOLOGY (CSB)

SINGAPORE-MIT ALLIANCE

NATIONAL UNIVERSITY OF SINGAPORE

2014

DECLARATION

I hereby declare that this thesis is my original work and it has been written by me in its entirety.
I have duly acknowledged all the sources of information which have been used in the thesis.

This thesis has also not been submitted for any degree in any university previously.

_____

Li Huipeng

14 January 2014

ACKNOWLEDGEMENTS

I would like to thank my supervisors Prof Hanry Yu (NUS) and Prof Jacob White (MIT), for supporting me during my PhD study. I thank Prof Hanry Yu for his constant guidance and immense support. His suggestions and comments have been very important in guiding me to shape the aims and contents of this thesis, introducing me from a physics background into biology, and developing fundamental abilities in scientific research. His ideas and efforts on team projects and matrix structure of the lab have created a friendly environment for multidisciplinary research, from which I benefitted immensely. I thank Prof Jacob White for his kind and patient guidance, and his support during my stay in MIT. His guidance on numerical analysis and dynamic simulation has helped me to develop computational methods for my research.

I would like to thank Dr Lisa Tucker-Kellogg for her guidance, ideas, discussions on my projects. I would like to thank her for her great patience in guiding me on learning biology, formulating projects, and the writing of my papers.

I would like to thank my SMA-CSB senior and colleague Lakshmi Venkatraman, for teaching me doing cell culture experiments, discussing with me and giving suggestions on my computational projects. I would like to thank my colleague Narmada, who taught me through various cell-based and biochemical assays, and gave me valuable suggestions on my experiments. I

would like to thank my SMA-CSB senior and colleague Wang Junjie, for all the valuable discussions.

Apart from that, I would like to thank my parents, who supported me in every aspect with their great love ever since. I would also like to thank all my colleagues, SMA-CSB classmates, and friends for their support and help.

Finally, I would like to thank Singapore-MIT Alliance for this opportunity and for the constant support and help throughout my PhD study.

TABLE OF CONTENTS

SUMMARY

Transforming growth factor β1 (TGF-β1) is one of the key cytokines involved in liver fibrosis. The level of TGF-β1 is significantly increased during liver fibrogenesis, and TGF-β1 is capable of increasing the deposition extracellular matrix (ECM) through different mechanisms. The importance of TGF-β1 in liver fibrosis makes it a potential target of anti-fibrotic therapies. Recently systems biology has been introduced to study TGF-β1 regulation in liver fibrosis [1,2]. A bistable model of the TGF-β1 activation network with multiple activators was built and validated in an in vitro model of liver fibrosis.

The TGF-β1 bistable activation model has explained the ability of PLS to negatively regulate TGF-β1 in a network system and cause a bistable switch of the level of TGF-β1. Understanding the TGF-β1 bistability and mechanisms of controlling the switch between its two steady states is important for designing anti-TGF-β1 therapies in liver fibrosis and other TGF-β1 related diseases. In this thesis, we use computational modeling and simulation to analyze the dynamics of TGF-β1 bistability. We aim to understand the mechanisms of how different factors could influence the steady states of TGF-β1 and the mechanisms of the switching of the bistable system.

In our first study of bistable TGF-β1 activation, we studied factors that could influence the switching of the steady states of TGF-β1. We extended the TGF-β1 bistable activation model to include calcium and Krüppel-like factor 2

(KLF2). We showed that increased levels of extracellular calcium would cause high levels of TGF-β1, resembling a fibrotic state, and increased levels of KLF2 would eradicate bistability and preclude the fibrotic steady-state. Simulations have also shown that activation of KLF2 was able to change the sign of feedback in the PLS − TGF-β1 − PAI1 loop.

The study of calcium and KLF2 revealed that the regulation of bistable systems should be considered on a system level. To achieve a general understanding of mechanisms of TGF-β1 bistable switch, in our second study, we used perturbation analysis to study the switch of the TGF-β1 bistable system under single and combination species perturbation. We perturbed individual and pairwise species to survey the additive and synergistic combinations in the TGF-β1 activation network model, and identified pairs of targets with strong synergistic effects. To account for the model uncertainty and parameter uncertainty in our predictions, we performed parameter perturbation analysis of combination species perturbation. Parameter perturbation analysis revealed positive correlation between synergism and relative robustness throughout the TGF-β1 activation network. Correlation between synergism and relative robustness was also seen when repeating the perturbation analysis on multiple bistable models from different areas of biology.

Overall, through computational modeling and analysis of network dynamics we achieved a deeper understanding of TGF-β1 bistability and the synergism

and robustness of TGF-β1 regulation. The insights generated from TGF-β1 bistable model in liver fibrosis contexts could have potential applicability to other TGF-β1 related diseases and other bistable systems.

LIST OF TABLES

LIST OF FIGURES

LIST OF SYMBOLS

A2M	alpha-2-macroglobulin
CI	combination index
CRN	chemical reaction networks
ECM	extracellular matrix
HGF	hepatocyte growth factor
HSCs	hepatic stellate cells
KLF2	Krüppel-like factor 2
LAP	latency associated peptide
LTGF-β1	latent transforming growth factor β1
MMPs	matrix metalloproteinases
ODE	ordinary differential equation
PAI1	plasminogen activator inhibitor-1
PLG	plasminogen
PLS	plasmin
ROS	reactive oxygen species
RR	relative robustness
scUPA	single chain urokinase plasminogen activator
ssHigh	steady state with high TGF-β1
ssLow	steady state with low TGF-β1
tcUPA	two chain urokinase plasminogen activator
TGF-β1	transforming growth factor β1
TIMPs	tissue inhibitors of metalloproteinases
TSP1	thrombospondin-1
uPA	urokinase plasminogen activator

CHAPTER 1: INTRODUCTION

1.1 Towards Systems Level Understanding of Biology

1.1.1 Systems biology

The remarkable contribution of molecular biology in the 20th century was the identification of the functions of numerous individual genes and proteins on the molecular level. However, it has long been known that biological systems are much more complex than the sum of their individual components. Aiming at systems level understanding of biology with molecular level resolution, the field of "systems biology" emerged around the year 2000 [3]. Since then, systems biology has become an active inter-disciplinary research area. It integrates genomics, molecular biology, high throughput experimental technology, computational modeling and simulation, and starts to reveal biological structures and functions at a new level.

To reach systems level understanding, the focus of systems biology has included (1) identification of structures of biological systems (e.g. identifying gene regulatory relationships, protein-protein interactions in signal transduction pathways, and gene regulatory networks); (2) analysis of behaviors of biological systems (e.g. the sensitivity of a system to perturbation of its components, and the transient behavior after perturbation); and (3) designing methods to control biological systems (e.g. controlling the level of important proteins in different diseases, and controlling the status of cells including apoptosis, differentiation). Due to the complexity of the problems

and the amount of data being generated, mathematical and computational methods have become an essential component of systems biology. To integrate and interpret data generated from different sources, mathematical and computational methods that have been developed and under development include but are not limited to, database integration methods, bioinformatics methods, dynamical systems methods, network analysis methods.

Ordinary differential equation (ODE) based chemical reaction networks (CRN) represents one of the most important computational methods in systems biology [4]. ODE-CRN translates a diagram of regulatory relationships between genes or proteins into a quantitative dynamic model. It not only enables the investigation of the dynamic behavior of biological systems based on previously discovered individual components, but also enables designing of in silico experiments to study the system behaviors under different conditions, which allows identification of methods to control the system. In the areas where individual components of complex networks were well studied, such as signal transduction cascades, metabolism pathways, and gene regulatory networks, ODE-CRN methods have been intensively applied.

1.1.2 Chemical reaction networks

A chemical reaction network is composed of a set of chemical reactions (Figure 1.1A). Chemical reaction networks typically contains three essential parts, species (or “nodes”, sometimes “components”), interactions (or

"structure", "topography") and parameters (including "reaction rate constants", "initial conditions", and other constants). The species of a chemical reaction network are usually represented by its biological name (gene name, protein name). For each chemical reaction, the direction of reaction is represented by an arrow pointing from reactants to products. The reactions rates are usually described by the **mass-action law**.

A

$\varnothing \xrightarrow{k1} A$ (*i*)

$A \xrightarrow{k2} B$ (*ii*)

$B \xrightarrow{k3} \varnothing$ (*iii*)

$C + D \xrightarrow{k4} E$ (*iv*)

$C + D \underset{k\_5}{\overset{k5}{\rightleftharpoons}} F$ (*v*)

B

(*i*) $r = k1\,[A]$

(*ii*) $r = k2\,[A]$

(*iii*) $r = k3\,[B]$

(*iv*) $r = k4\,[C]\,[D]$

(*v*) $r_f = k5\,[C]\,[D]$, $r_r = k\_5\,[F]$

C

	(a)	(b)	(c)	(d)
reactions	$A \underset{kp}{\overset{kd}{\rightleftharpoons}} \varnothing;$	$B \xrightarrow{kp} A;$ $A \xrightarrow{kd} \varnothing;$	$C + D \xrightarrow{kb} E;$	$C + D \underset{k\_b}{\overset{kb}{\rightleftharpoons}} F;$
ODEs	$d\frac{[A]}{dt} = kp - kd\,[A];$	$d\frac{[A]}{dt} = kp\,[B] - kd\,[A];$	$d\frac{[E]}{dt} = kb\,[C]\,[D];$ $d\frac{[C]}{dt} = -kb\,[C]\,[D];$ $d\frac{[D]}{dt} = -kb\,[C]\,[D];$	$d\frac{[F]}{dt} = kb\,[C][D] - k\_d\,[F];$ $d\frac{[C]}{dt} = -kb\,[C][D] + k\_d\,[F];$ $d\frac{[D]}{dt} = -kb\,[C][D] + k\_d\,[F];$

Figure 1.1: Chemical reaction networks and their ODE form. (A) An example chemical reactions network with six species (i.e. [**A**,**B**,**C**,**D**,**E**,**F**]), five reactions (i.e. i-v) and six rate constants (i.e. [**k1**,**k2**,**k3**,**k4**,**k5**,**k_5**]. (B) The mass-action reaction rate (**r**) of the network in (A), $\mathbf{r_f}$ means "forward" rate, and $\mathbf{r_b}$ means backward rate. (C) Several simple network models and their ODE forms. (a) degradation and constant production. (b) degradation and production by upstream molecules. (c) irreversible binding reaction between two substrates. (d) reversible biding reaction between two substrates.

The mass-action law assumes reactions happen in a confined space (i.e. the volume of the reaction is fixed), and the number of molecules for each species is large enough so that the concentration can be treated as a continuous

variable. The mass-action law states that “the rate of a chemical reaction is proportional to the product of the concentration of the reactants”. For example, in Figure 1.1B, the reaction rate of reaction (ii) can denoted as k2[A]; and the reaction rate of reaction (iv) can be denoted as k4[C]*[D]. In these terms, k2 and k4 are constants of proportionality, and are also called (mass action) rate constants. Depending upon the number of reactants, the reaction rates can be of zero order, first order, or second order.

The mass-action law allows us to build mathematical models of chemical reaction networks in the form of ordinary differential equations (ODEs). A chemical reaction network composed of N species can generate a system of N ordinary differential equations, with each equation describing the temporal dynamics of the concentration of one species. The time derivative of the concentration of each species equals to the sum of the mass-action-law reaction rates from all reactions this species is involved in. With a set of initial concentrations of all species, the dynamics of a network can be simulated.

Figure 1.1C shows several simplest chemical reaction networks, and their ODE forms. These simplest networks are basic modules of much more complicated networks. For example, in signaling transduction network models, the production and degradation of proteins are mainly modeled in forms of model (a) if there is a constant production rate, or equation (b) if it is dependent upon some upstream species. The equation (c) and (d) are the general form of two substrate reactions, either reversible (c) or irreversible (d).

1.1.3 Analysis of dynamics of network models

The ODE form of chemical reaction networks makes complex dynamic analysis possible. With an ODE model of a network, one can analyze the steady state behavior and the transient dynamics of the system. ODE models also allows us to analyze the dependence of the behavior of the system on certain rate constants (i.e. bifurcation analysis) and the behavior of the systems when there is random change in the whole set of rate constants (i.e. sensitivity/ robustness analysis).

Steady State Analysis:

Steady state behavior is an important type of long term asymptotic behavior of biological network models. A network model reaches a steady state when the concentrations of all species make the overall reactions rates (time derivative) of each species zero (Figure 1.2A-B). The list of concentrations of all species is called a steady state (vector) of the system. A long term reachable steady state is called a stable steady state. When a system is at its stable steady state, small perturbations can cause some transient effects but won't change the long term steady state of the system. The other type of steady state is an unstable steady state. Although concentrations of unstable steady states also generate zero net reaction rates, tiny perturbations from it would lead the system further away. Therefore, an unstable steady state is long term unreachable.

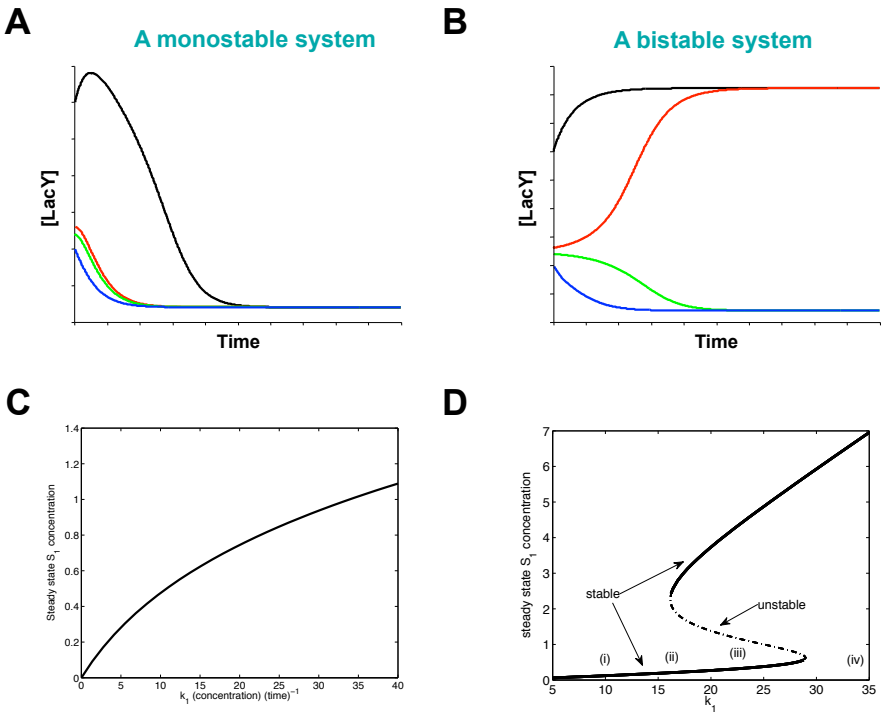

Figure 1.2: Dynamics of network models. (A) Illustration of the concentration of one species approaching steady state in monostable system [5]. (B) Illustration of the concentrations of one species approaching steady states in bistable system [5]. (C) Illustration of continuation diagram [6]. (D) Illustration of bifurcation diagram [6].

Systems that have only one stable steady state are called monostable systems (Figure 1.2A), while systems with more than one stable steady states are called multistable systems. Specifically, systems with two stable steady states are called bistable systems (Figure 1.2B). Bistability is of great importance in systems biology since many biological systems show bistable behavior. Bistability produces important biological behaviors such as allowing diverse inputs to converge toward a single binary (yes/no) decision, "remembering" a previously chosen steady state over time, remaining at the same steady state in

the presence of random noise, and switching between two states with ultrasensitive response to a particular stimulus. Some biological effects are binary at the level of single cells but graded-response for a population of cells, and some bistable effects have binary output even for a population of cells [1]. Biological implications of bistability will be discussed in detail in Chapter 3.

Bifurcation Analysis:

The steady state concentrations of a system usually changes when there is a change in the rate constants. The diagram that depicts a steady state concentration versus the value of a rate constant is called a continuation diagram (Figure 1.2C). Sometimes, the variation in model parameters can cause a qualitative change in the model behavior, for example the number of steady states. The values of the parameters where such qualitative changes occur are called bifurcation points. A continuation diagram containing bifurcation points is called bifurcation diagram (Figure 1.2D).

Bifurcation analysis suggests the robustness of the behavior of the system. Systems with parameter values far from bifurcation points are less likely to have qualitative change in behaviors upon perturbation. While systems near the bifurcation points tend to have dramatic change in their behaviors.

Robustness Analysis:

Robustness is a ubiquitous property of biological systems, which means the ability of maintaining functions under external disturbances. When building a

network model of a certain biological system, robustness analysis is necessary for evaluating the model's validity and investigation of the robustness of the real biological system.

Parameter sensitivity analysis is a widely used method of robustness analysis. Parameter sensitivity analysis evaluates the dependence of system behavior on the whole parameter set. Parameter sensitivity analysis can be divided into two types, global sensitivity analysis and local sensitivity analysis. Global sensitivity analysis deals with parameter variations in a wide range. It usually applies a sampling strategy to the whole parameter space and use statistics for analysis. Local sensitivity analysis deals with small parameter variations, and it usually employs analytical or numerical methods for sensitivity quantification.

1.1.4 Network models for disease and therapy

ODE based network models have been used to study various biological systems, including Epidermal Growth Factor (EGFR) signaling [7], Extracellular-signal-regulated kinase (ERK) signaling [8], Akt signaling [9]. Many of these biological networks are involved in disease contexts and are becoming an important tool for drug target identification. For example, Wnt signaling and the MAPK signaling pathway have been used to identify potential drug targets for embryonic development, cancer [10,11].

Another important potential value of network models is the designing of combination therapy [10,12]. Due to the large number of nodes in many biological networks, and the lack of proper chemical reagents to target them, it is often impossible to evaluate all possible target combinations experimentally. Even in cases when experimental exploration is possible, the cost can be extremely high. However, when a mathematical network model has been validated in a disease context, it can be used for virtual screening of all types of combination targeting strategies. The dose effect of each drug and their combination effect (synergy, additivity, antagonism) can be evaluated computationally with much lower cost (see Chapter 3 and Figure 3.S1 for more details on the definition of synergy, additivity and antagonisms).

Recently, mathematical models have been applied to the field of liver fibrosis [1,2]. These studies applied the dynamic systems modeling method to study the molecular networks underlying liver fibrosis. These studies identified an important activation network of a key regulator of liver fibrosis, **transforming growth factor β1** (**TGF-β1**). These studies laid the foundation for network level analysis of TGF-β1 regulation, and create opportunity for in silico exploration of combination targeting of TGF-β1 for the treatment of liver fibrosis.

1.2 Towards Systems Level Understanding of TGF-β1 regulation in liver fibrosis

1.2.1 Liver fibrosis and TGF-β1

Liver fibrosis is characterized by the accumulation of extracellular matrix (ECM), especially collagen caused by various chronic injuries, including hepatic B virus (HBV), hepatic C virus (HCV), alcoholic liver disease and NASH [13]. The late stage of liver fibrosis is called cirrhosis. Hepatic stellate cells (HSCs) are the main producers of ECM during liver fibrosis. In a normal state, HSCs store vitamin A and reside in the space of Disse. HSCs get activated during liver injury and activated HSCs show high rate of proliferation, and ECM production (Figure 1.3) [14].

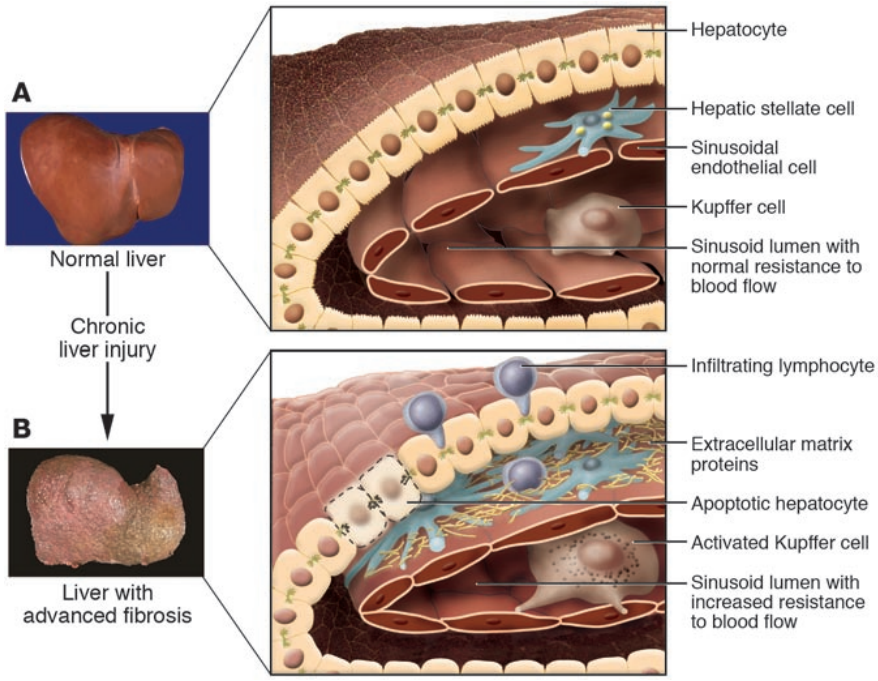

Figure 1.3: Changes of liver during liver fibrosis. (A) Normal liver. (B) Fibrotic liver. [13].

Many cytokines and growth factors are involved in the process of liver fibrosis [13]. TGF-β1 is one of the most important of them (Figure 1.4) [15]. It has been shown that TGF-β1 can increase ECM protein levels by both enhancing their production through cell signaling and reducing their degradation through the regulation of the level of MMPs and TIMPs. TGF-β1 has been shown to be able to activate HSCs and enhance their ECM production level. In the liver, TGF-β1 is able to down-regulate proliferation of hepatocyte and induce apoptosis of hepatocytes. These properties make TGF-β1 a potential target of anti-fibrotic therapy [16]. Several anti-TGF-β1 strategies have been designed for the treatment of liver fibrosis, including hindering TGF-β1's binding to receptors, block extracellular activation of TGF-β1, interfering downstream TGF-β1 signaling.

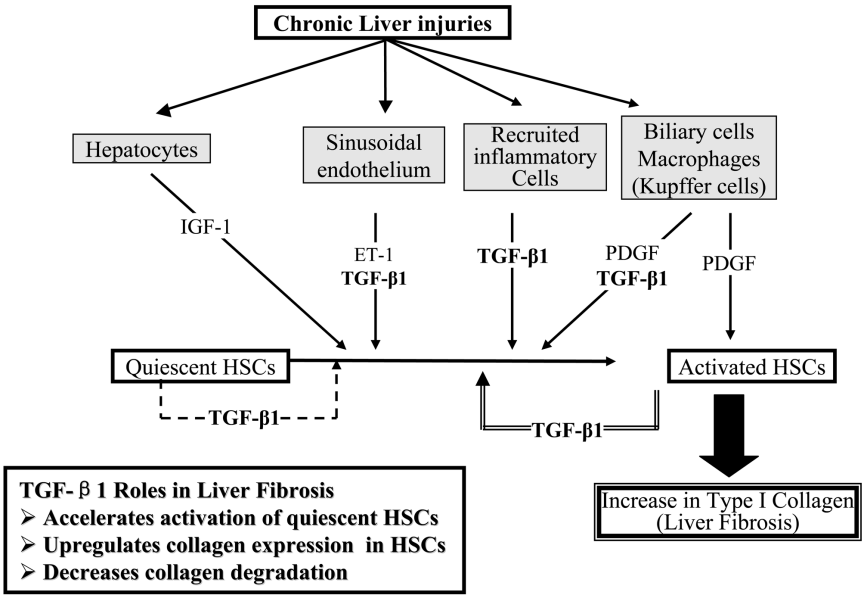

Figure 1.4: Roles of TGF-β1 in liver fibrosis. [17].

TGF-β1 is secreted and stored in extracellular space in an inactive form, called latent-TGF-β1 (LTGF-β1) [18]. LTGF-β1 is prevented from binding to TGF-β1 receptors by the Latency Associated Peptide (LAP). TGF-β1 latency gives opportunity for regulation of TGF-β1 activity in different cellular conditions. A number of activators of TGF-β1 have been identified, including integrin, pH, reactive oxygen species (ROS), proteases and metalloprotease, and thrombospondin-1 (TSP1) (Figure 1.5).

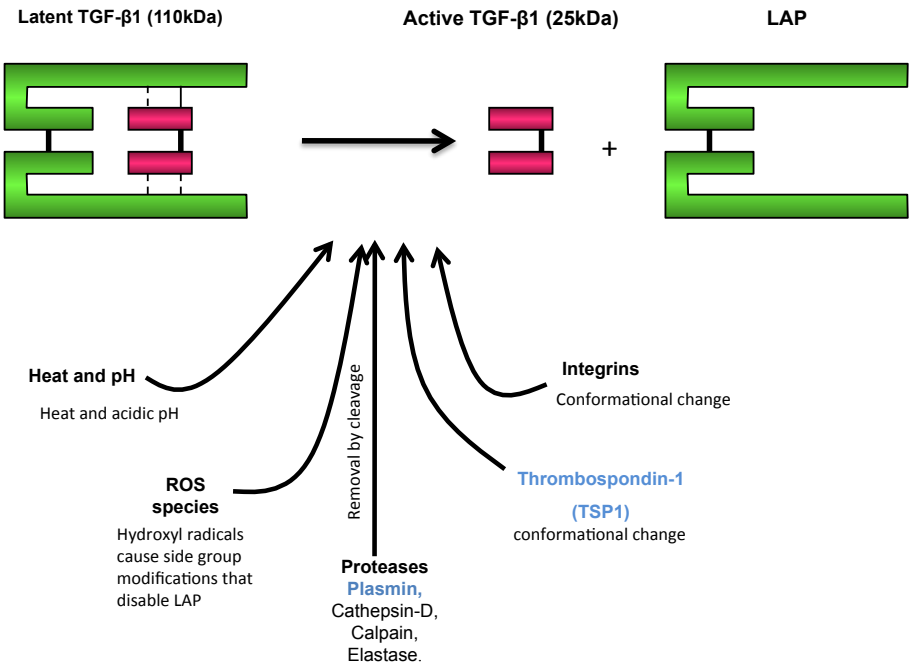

Figure 1.5: TGF-β1 latency and its activation by a number of activators.

1.2.2 Activation of TGF-β1 by plasmin (PLS) and thrombospondin-1 (TSP1)

Plasmin (PLS) and TSP1 are two major activators of TGF-β1 in the liver. TSP1 is a matrix glycoprotein produced by many cell types. In a fibrotic liver, TSP1 is mainly produced by activated HSCs. TSP1 activates TGF-β1 by conformational change of LTGF-β1 and releasing active TGF-β1. It has been shown that TSP1 is able to activate TGF-β1 in various contexts [19,20]. In liver fibrosis, TSP1 is used as a marker of fibrosis due to the strong correlation of TSP1 level and fibrosis progression in vivo. Furthermore, blocking the TSP1 and TGF-β1 interaction has been shown to be able to prevent liver fibrosis in animal studies [21].

Plasmin is a serine protease that degrades many proteins. In the liver, plasmin is mainly produced by hepatocytes. Plasmin activates TGF-β1 by cleavage of LAP in the LTGF-β1 complex [22]. However, despite the evidence of activation of TGF-β1 by plasmin in a cell free system, plasmin has been shown to down-regulate TGF-β1 activation in vitro and in vivo. A number of studies showed plasmin has anti-fibrotic effects, partly due to its anti-TGF-β1 activation property [23,24].

1.2.3 Bistable TGF-β1 activation by PLS and TSP1 in liver fibrosis

The controversial effect of PLS on TGF-β1 in a cell free system and in vivo suggests that TGF-β1 activation should be discussed on a system level, taking into account the effects of multiple regulators. Venkatraman et al have studied TGF-β1 activation in an in vitro model of liver fibrosis by considering both the PLS and TSP1 activation pathway [1]. A mathematical model of TGF-β1 activation by PLS and TSP1 was built to help understand the effect of anti-TGF-β1 effect of PLS. This model includes the activation of TGF-β1 by PLS and TSP1, and also includes the feedback from TGF-β1 to PLS and TSP1. The feedback from TGF-β1 to PLS is a negative feedback since TGF-β1 can increase the expression of plasminogen activator inhibitor-1 (PAI1). The feedback from TGF-β1 to TSP1 is a positive feedback since TGF-β1 can increase the expression of TSP1. This model includes the mutual antagonism

between PLS and TSP1 as well, meaning PLS can cleave TSP1 and TSP1 can inhibit the activity of PLS (Figure 1.6A).

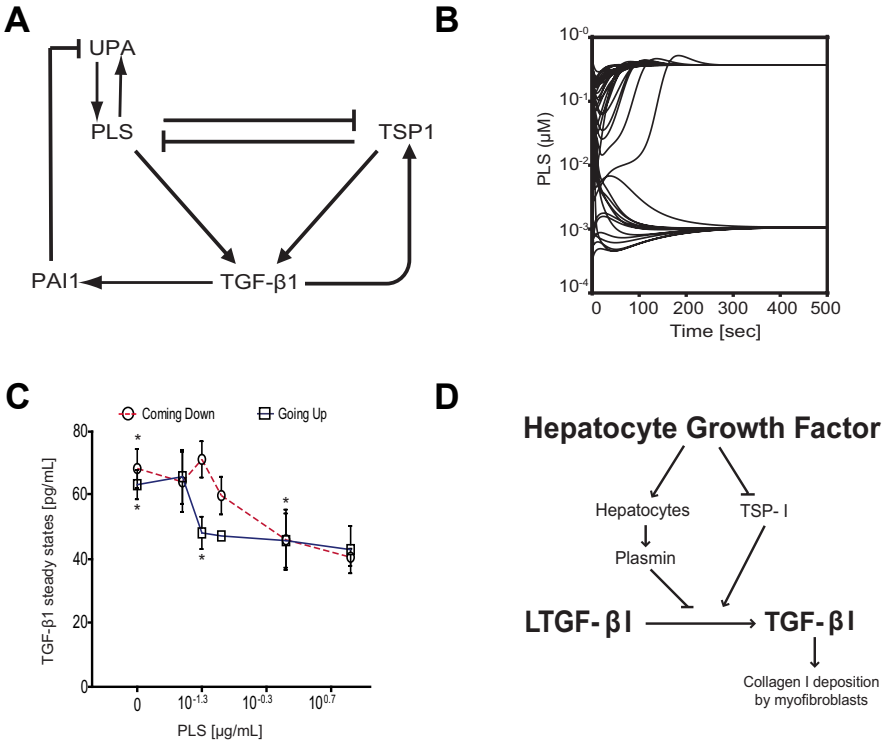

Figure 1.6: Bistable TGF-β1 activation by PLS and TSP1 in liver fibrosis. (A) Schematics of the main interactions between species of the model [1]. (B) Bistable behavior of the computational model [1]. (C) Bistability of TGF-β1 in hepatocyte-HSC co-culture model [1]. (D) Schematic diagram of possible anti-fibrotic effects of HGF on TGF-β1 activation [2].

The model shows bistability of TGF-β1 activation, which means the system can be stabilized at two distinct steady statea, a steady state with high TGF-β1 activation, and a steady state with low TGF-β1 activation. The bistability of

TGF-β1 activation has been shown in both computer simulation and in vitro experiments (Figure 1.6B-C).

The model of TGF-β1 activation by PLS and TSP1 has also been used to explain the anti-fibrotic effect of the hepatocyte growth factor (HGF) [2]. HGF is a growth factor that regulate multiple cellular behaviors, including cell growth, motility, morphogenesis. HGF has been shown to be abnormally low in liver fibrosis [25] and over-expressing HGF showed remarkable anti-fibrotic effect in the liver [26,27]. In Narmada et al's work, HGF was shown to be able to increase the level of PLS and inhibit the activity of TSP1 (Figure 1.6D). According to the model built by Venkatraman et al, both of these two effects can trigger the down-regulation of TGF-β1 activity. Indeed, Narmada et al have shown that HGF can down-regulate the level of active TGF-β1 and also collagen type I (the major component of ECM in fibrotic liver) in a hepatocyte-HSC co-culture system.

1.3 Thesis Overview

Previous work on modeling of TGF-β1 activation and the regulation of TGF-β1 by HGF laid the foundation of studying TGF-β1 regulation on a system level. Based on the TGF-β1 activation model, it is possible to study the regulation of TGF-β1 on a system level. Analysis of the dynamics of the TGF-β1 activation network model would help us identify regulatory mechanisms of

TGF-β1 by different regulators, and direct the design of methods to control the level of TGF-β1.

One interesting problem would be how different regulators beyond PLS, TSP1, and HGF would affect the TGF-β1 bistability and its network level behavior. Another interesting problem would be how to design and select combination targeting strategies of anti-TGF-β1 therapy. In this thesis, we first investigated how different regulators can affect the bistability of the model, and how the environment can change the sign of the feedback loops within the network. We then discussed strategies of controlling the level of TGF-β1, focusing on the combination targeting strategy to induce a bistable switch of the TGF-β1 network model.

Chapter 2 will discuss how literature mining, computational modeling, and experimental validation yields deeper understanding of the regulation of bistable TGF-β1 activation, with implications for potential anti-TGF-β1 strategies and network level feedback behaviors.

Chapter 3 will discuss combination perturbation problem of bistable networks in general. When studying the combination targeting problem of the TGF-β1 network model, a qualitative correlation between synergy and robustness of drug doses was observed. Further investigation on multiple bistable models suggests that this property could be a general property of many bistable models.

Chapter 4 will conclude the work in chapter2 and chapter 3.

Chapter 5 will discuss some potential future work, including non-monotonic transition behavior as an important property of bistable systems, and the experimental study of combination targeting of TGF-β1 activation.

CHAPTER 2 : COMPUTATIONAL MODELING OF BISTABLE TGF-β1 ACTIVATION: CASE STUDIES WITH CALCIUM AND KLF2 SHOW REGULATION OF TGF-β1 AND A SWITCH BETWEEN POSITIVE AND NEGATIVE FEEDBACK

2.1 Overview

This chapter focuses on how different regulators beyond PLS, TSP1, and HGF would affect the TGF-β1 bistability and its network behavior. We will see how literature mining can suggest potential regulators of our TGF-β1 activation model. We will expand our TGF-β1 model to incorporate the effects of those regulators outside the scope of the model. Analysis of the dynamics of the model through simulation will suggest important properties of TGF-β1 regulation networks.

2.2 Abstract

A bistable switch has recently been found to regulate the activation of transforming growth factor-β1 (TGF-β1). An ordinary differential equation (ODE) model was published showing that the net activation of TGF-β1 depends on the balance between two antagonistic sub-pathways. Here we model perturbations that affect both sub-pathways, and simulate how their propagated effects impact the TGF-β1 system.

We extended the model to include calcium and Krüppel-like factor 2

(KLF2), both regulators of Thrombospondin-1 (TSP1) and Plasmin (PLS). Increased levels of extracellular calcium, which alters the TSP1-PLS balance, would cause high levels of TGF-β1, resembling a fibrotic state. KLF2, which suppresses production of TSP1 and plasminogen activator inhibitor-1 (PAI1), would eradicate bistability and preclude the fibrotic steady-state. Finally, the loop PLS − TGF-β1 − PAI1 had previously been reported as negative feedback, but the model suggested a stronger indirect effect of PLS down-regulating PAI1 to produce positive (double-negative) feedback at fibrotic state. Further simulations showed that activation of KLF2 was able to restore negative feedback in the PLS − TGF-β1 − PAI1 loop.

We conclude that factors such as calcium or KLF2, that can affect both the TSP1 sub-pathway and PLS sub-pathway, could have a greatly amplified effect on the feedback behavior.

2.3 Background

Transforming growth factor-β1 (TGF-β1) is a cytokine with broad importance for cancer, liver cirrhosis, and other diseases. We previously developed a model of TGF-β1 activation, and the model successfully predicted that TGF-β1would exhibit bistability in cells [1]. The model captures multiple pathways with positive and negative effects towards TGF-β1 and its activators. The full model is described in Figure 2.1 (Figure 2.1, black arrows). To summarize this model, TGF-β1 is activated by plasmin (PLS) or

thrombospondin-1 (TSP1), each having its own feedback mechanisms [1]. PLS feedback occurs because PLS activates TGF-β1 [18,22], and then TGF-β1 upregulates plasminogen activator inhibitor-1 (PAI1), which is an inhibitor of plasminogen activation [28,29]. These effects form a negative feedback loop between TGF-β1 and PLS. In contrast, TSP1 feedback occurs because TSP1 activates TGF-β1, and TGF-β1 upregulates TSP1 [19,30,31], creating a positive feedback loop between TGF-β1 and TSP1. There is also mutual antagonism between PLS and TSP1 [32,33], which pushes the system towards either a "PLS-predominant" steady state, or "TSP1-predominant" steady state. The "PLS-predominant" steady state (ssP) has moderate levels of TGF-β1 due to negative feedback [1]. In contrast, the TSP1-predominant steady state (ssT) achieves a higher level of TGF-β1 activation due to positive feedback [1]. Venkatraman et al. have shown that introducing extra PLS into a TSP1 dominant system would switch the balance between PLS and TSP1, thus inducing a decrease in the level of active TGF-β1.

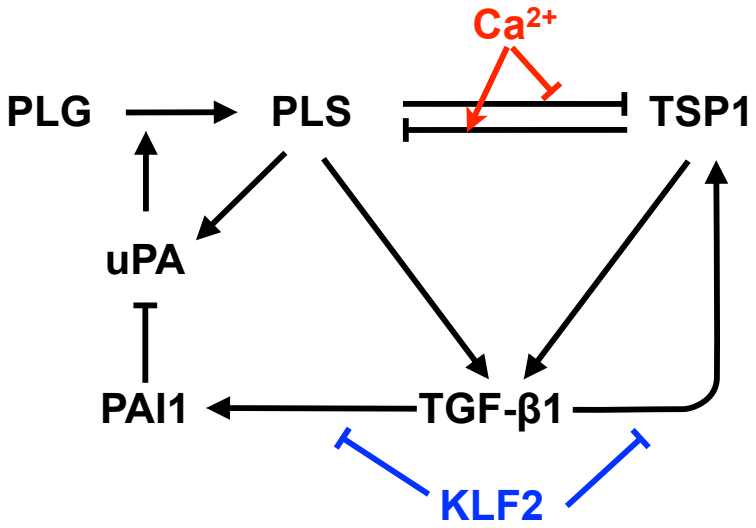

Figure 2.1: TGF-β1 bistable activation model. Black arrows represent the reactions from [1]. Red arrows represent the effects of calcium on the PLS-TSP1 interaction. Blue arrows represent the effects of KLF2 on PAI1 and TSP1 production. uPA is urokinase plasminogen activator, and PLG is plasminogen.

In the current study, we explore some possible triggers that could influence the bistable transition, and we discover that the bistable transition is correlated with a transition in the feedback behavior of the network. A literature search yielded two factors that could regulate both PLS and TSP1, calcium [34,35] and Krüppel-like factor 2 (KLF2) [36-38]. Calcium has been found to enhance the inhibition of the activity of PLS by TSP1, and suppress the cleavage of TSP1 by PLS [34,35]. KLF2 have been found to cause significant suppression of TSP1 and PAI1 [37,38], meaning that KLF2 could regulate both PLS and TSP1 sub-pathways of TGF-β1 activation. Simulation showed how calcium and KLF2 could alter the activation of TGF-β1 by influencing the PLS-TSP1 interplay. Simulation of the KLF2 also revealed that there could

be a qualitative change in the behavior of some feedback loops in the network.

2.4 Results

2.4.1 Calcium would promote the steady state with high TGF-β1 activation

We built the low and high calcium variants of the model by considering the potential effects of calcium on the PLS-TSP1 interaction (see Methods, Figure 2.1 red arrows). Three parameters for the calcium effect were not known quantitatively and were estimated (see Methods). In Figure 2.2A-B, we simulated the low calcium model and the high calcium model over time with 27 total initial configurations. These 27 configurations were combinations of 3 initial concentrations for each of TGF-β1, TSP1, and plasmin, the ssT level, ssP level, and the mean level of ssT and ssP ($27 = 3^3$). The initial concentrations of other species were set to the average of their two steady state levels, (i.e., 0.5ssT + 0.5ssP). In the low-calcium model, all trajectories converged to ssP with low TGF-β1, but in the high-calcium model, several of the initial configurations converged to ssT with high TGF-β1. To generalize our understanding of this effect, we plotted the boundary (the separatrix, Figure 2.2C) between the initial configurations that caused convergence toward ssT (red) and the initial conditions that caused convergence toward ssP (blue). Initial concentrations were constants for all species other than PLS and TSP1. By comparing the separatrix of the low calcium model (dot) and the high calcium model (circle), we observe a shift of the separatrix toward the

blue (ssP) region. This means the red (ssT) region is enlarged in a high calcium environment (arrow 3). As expected, calcium tips the balance between PLS and TSP1 to achieve a significant effect on steady state of TGF-β1 activation.

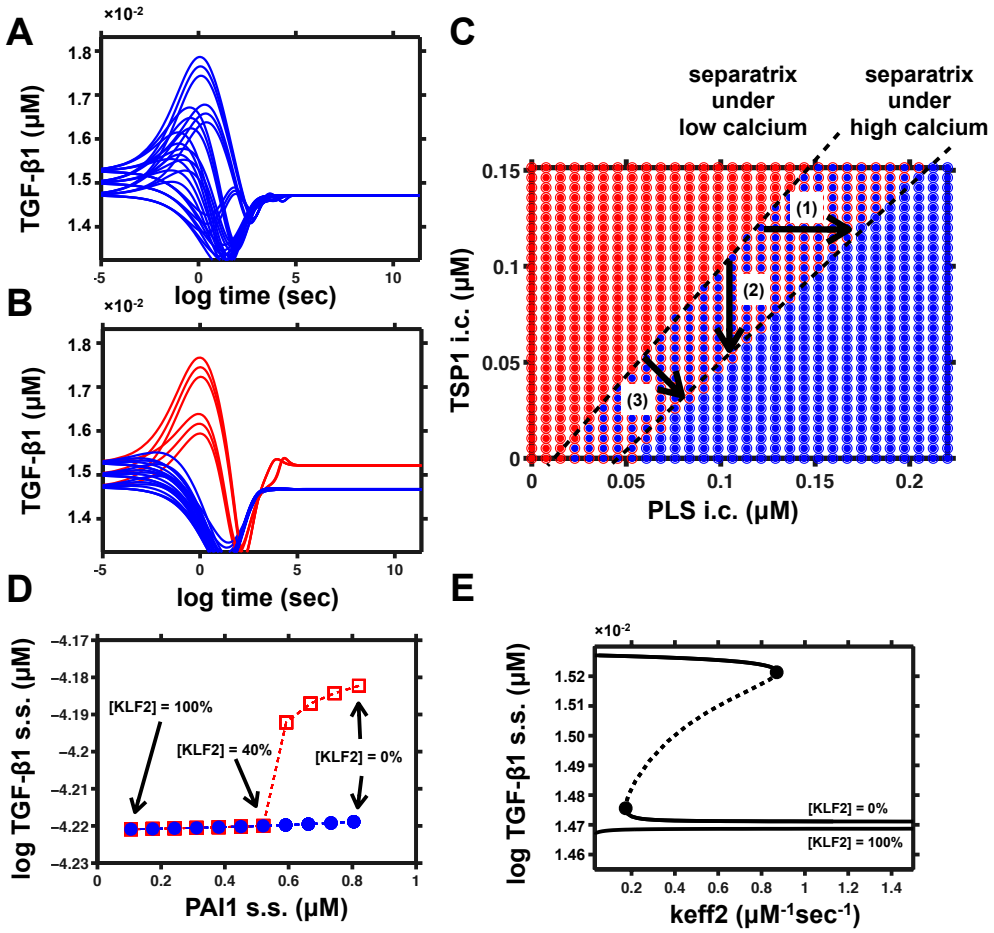

Figure 2.2: Calcium and KLF2 have potential influence on the steady state of TGF-β1 activation. (**A**) Time dependent curves of TGF-β1 with a given set of initial conditions, under low calcium condition. Blue represents that the system converges to the low TGF-β1 activation steady state (ssP). (**B**) Time dependent curves with the same set of initial conditions as in (**A**) under high calcium condition. Red represents that the system converges to the high TGF-β1 activation steady state (ssT). (**C**) The steady state of the system with different combinations of TSP1 initial concentration and Plasmin initial concentration. Red color represents a high TGF-β1 activation steady state (ssT), while blue color represents a low TGF-β1 activation steady state. Dot

represents a low calcium condition, while circle represents a high calcium condition. (**D**) Two steady states of TGF-β1 and PAI1 under different levels of KLF2. The red square represents the high TGF-β1 activation steady state, while the blue dot represents the low TGF-β1 activation steady state. (**E**) Bifurcation analysis under KLF2 low and KLF2 high conditions. Solid sections represent the stable steady states. Dotted sections represent the unstable steady state. Black dots represent the bifurcation point of the system.

2.4.2 KLF2 would eliminate the steady state with high TGF-β1 activation

KLF2 is a transcription factor studied extensively in atherosclerosis and fibrosis, and previous studies of KLF2 signaling showed TSP1 and PAI1 (plasminogen activator inhibitor-1) to be two of its most strongly affected targets [37,38]. To study how KLF2 would affect bistable activation of TGF-β1, variants of the TGF-β1 activation model were built as described in methods (Figure 2.1 blue arrows). We built a model called "100% KLF2" that downregulated the TSP1 production and PAI1 production rates, proportional to the published effects of KLF2 on the mRNA levels of TSP1 (-7.8 fold) and PAI1 (-7.4 fold). This is a strong effect, so we also built models with 90%, 80%, … 10%, and 0% of the KLF2 effects on the TSP1 and the PAI1 production rates. Each model in the series was simulated to obtain the steady state concentrations. When a dynamical system is bistable, its two steady states are commonly obtained by simulating the model twice, once starting from each side of the separatrix boundary (for example, initializing the system with opposite extreme levels of TGF-β1). For our series of models, the steady states obtained after initialization with high TGF-β1 (resembling ssT) were

plotted with open red boxes, and the steady states obtained after initialization with low TGF-β1 (resembling ssP) were plotted with solid blue circles (Figure 2.2D). Models for each level of KLF2 were plotted in terms of PAI1 and TGF-β1 steady states (with KLF2 levels decreasing from left to right). For models with KLF2 ≥ 40%, the open red boxes fell at the same points as the solid blue circles, indicating they are monostable. For models with KLF2 ≤ 30%, the red open boxes were distinct from the blue circles, indicating two steady states. For KLF2 levels from 0% to 100% (right to left), the low TGF-β1 steady state (blue dots) remained almost constant, while the high TGF-β1 steady state (red boxes) merged with the low TGF-β1 steady state in an ultrasensitive manner when the KLF2 effect increased from 30% to 40%.

Bifurcation analysis studies how parameter change affects the qualitative behavior and the steady states of a system [39]. A bifurcation plot allows us to see all the equilibria of the system and how the equilibria vary with change of KLF2 levels and other rate parameters. We chose one parameter named "keff2" to show the steady state behavior of the low KLF2 and high KLF2 system. "Keff2", the enzymatic efficiency of plasmin, is one of many rate parameters that affect the overall bistability of the system. Figure 2.2E shows the bifurcation plot for the 0% KLF2 model and the 100% KLF2 model with respect to the parameter "keff2". Solid lines represent the stable steady states of the system (ssP or ssT). Dotted lines represent one unstable steady state between the two stable steady states, which is not achievable through

simulation. Black circles represent two limit points in the bifurcation curve, which separates the monostable regime and bistable regime. Bifurcation analysis confirmed that the system with 0% KLF2 retained bistability (an "S-shaped" curve in Figure 2.2E) while the system with 100% KLF2 was monostable.

2.4.3 The bistability of the system correlates with the sign of the PLS-PAI1 feedback loop

Positive and negative feedback loops are ubiquitous in biological systems [40], and necessary for many functions [41,42]. The TGF-β1 activation network is composed of multiple overlapping feedback loops, including two feedback loops between PLS and PAI1. One obvious loop is the negative feedback loop PLS→TGF-β1→PAI1⊣PLS, which is frequently cited [43-47]. A less obvious loop is PLS⊣TSP1→TGF-β1→PAI1⊣PLS, with two inhibitory effects, meaning positive feedback (See Figure 2.3A-B). Interestingly, experiments have already observed two opposite behaviors of PLS towards TGF-β1 and PAI1 [48-50], giving indirect evidence for the possibility of both positive and negative feedback loops involving PLS, TGF-β1, and PAI1.

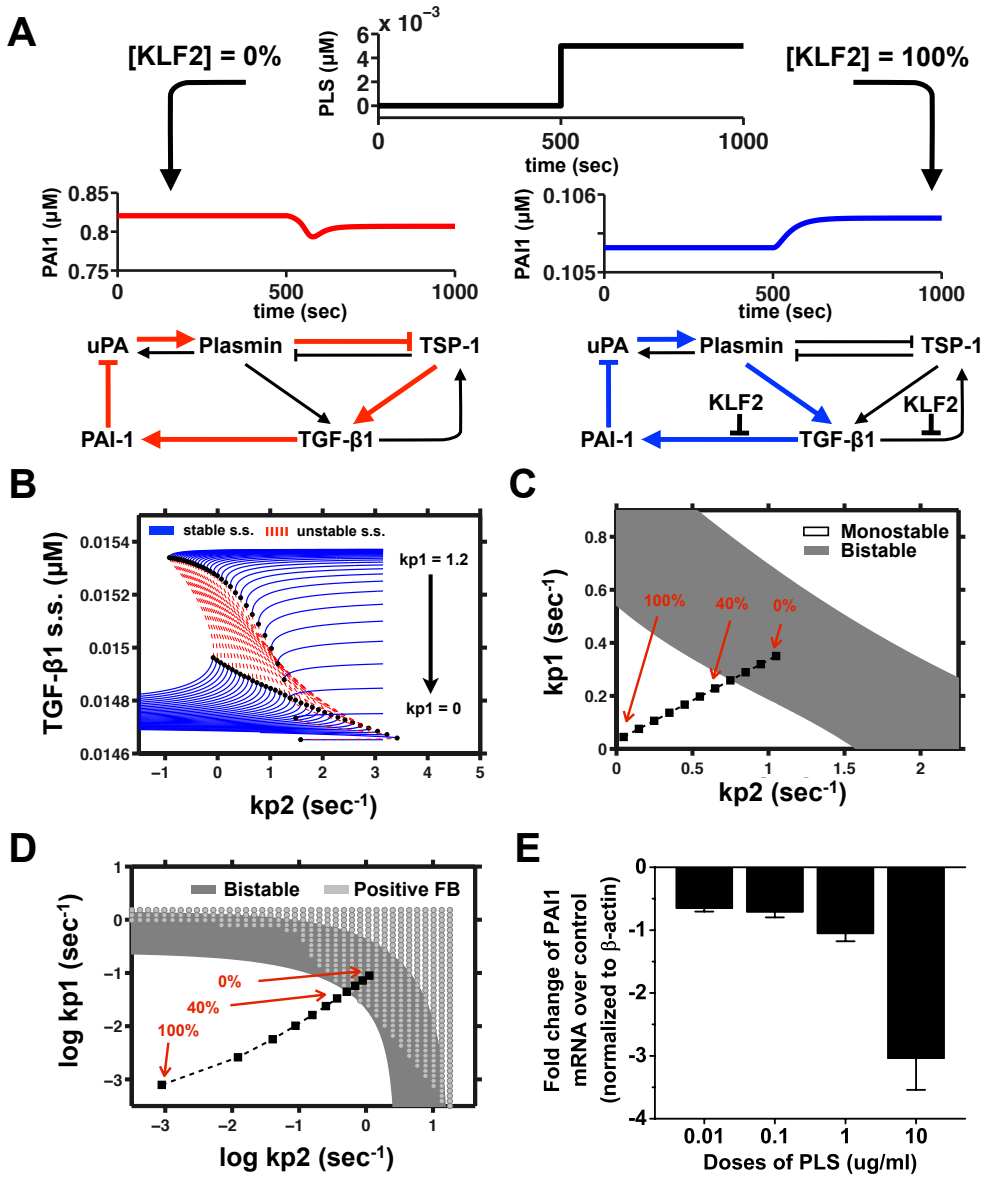

Figure 2.3: The bistability of the system correlates with the sign of the PLS-PAI1 feedback loop. (A) We designed an exogenous addition of PLS into the system using a step function for the level of PLS over time (top curve panel in black). Stimulating the TGF-β1 activation model with exogenous PLS caused two different effects *in silico*, depending on the KLF1 status. In the absence of KLF2 (red curve on left), the stimulus caused positive (double-negative) feedback between PAI1 and Plasmin, which can occur via the red arrows shown. In the presence of KLF2 (blue curve on right), exogenous PLS treatment caused a positive effect on PAI1 and the negative feedback loop (blue arrows) was restored. (B) *kp2*-bifurcation diagram for a series of *kp1* values. Solid blue represents stable steady states. Dotted red represents unstable steady state. Black dots represent limit points on bifurcation curves. Intervals between the *kp2* values of two limit points on bifurcations curves

with continuous *kp1* will indicate the bistable regions on *kp1-kp2* plane (i.e. combinations of *kp1* and *kp2* values that make the system bistable). (C) Bistable region and KLF2 levels on *kp1-kp2* plane. White color indicates the monostable region. Gray color indicates the bistable region. Different levels of KLF2 are represented by black squares. System with 0% KLF2 lies within bistable region, while as the level of KLF2 increases, the system gradually shifts towards a monostable region. (D) Bistable regions, PAI1-PLS positive feedback region and KLF2 levels on *kp1-kp2* plane. Light gray dots indicate the region in which the system has positive feedback behavior between PAI1 and PLS. Dark gray represents the bistable region. System with 0% KLF2 lies in the region with both bistability and PAI1-PLS positive feedback. As the level of KLF2 increases, the system gradually shifts towards a monostable region with PAI1-PLS negative feedback. Notice that the large overlap between bistability and PAI1-PLS positive feedback could suggest potential correlation between bistability and PAI1-PLS positive feedback. (E) Experimental testing of the PAI1-PLS feedback in a bistable system. Different levels of PLS were added into a co-culture model of hepatocytes and HSC-T6, where bistability has been verified [1]. Level of PAI1 mRNA were measured through RT-PCR. Data showed that PLS could down-regulate PAI1 gene expression, indicating a positive (double-negative) feedback between PLS and PAI1.

To characterize the feedback between PLS and PAI1 in this network, we plotted feedback behavior in both low KLF2 (0%) and high KLF2 (100%) models (Figure 2.3A). Since PAI1 (plasminogen activator inhibitor-1) is antagonistic towards PLS, the sign of the PLS-PAI1 feedback loop is determined by the response of PAI1 to PLS. We used a stepwise PLS input (black curve) to perturb both the low (%0) KLF2 model and the high (100%) KLF2 model and we simulated the response of PAI1. The low KLF2 model showed a decrease in the level of PAI1, which means that the overall PLS-PAI1 feedback is dominated by the PLS⊣TSP1→TGF-β1→PAI1⊣PLS double negative (positive) feedback loop. The high KLF2 model showed an increase in the level of PAI1, which means that the overall PLS-PAI1 feedback is

dominated by the PLS⊣TSP1→TGF-β1→PAI1⊣PLS negative feedback loop.

It was interesting to observe in simulation that KLF2 not only was able to eliminate one of the steady states and turned the system into monostable, but also able to change the sign of the PLS-PAI1 feedback loop. To further characterize the effect of KLF2 on the system and discuss the reason behind it, we plotted the 2d bistable region of the system in the *kp1-kp2* phase plane (Figure 2.3C). We did this through equilibrium continuation of *kp2* for a series of *kp1* values (Figure 2.3B). In our model, KLF2 is represented as a combination of fold changes of *kp1* and *kp2*, therefore, KLF2 levels can be represented as a series of points in the *kp1-kp2* phase plane (Figure 2.3C). It can be seen on Figure 2.3C that the KLF2 point is moving out of the bistable region when KLF2 increases from 0 to 100%. We then analyzed the sign of PLS-PAI1 feedback in this *kp1-kp2* phase plane. Interestingly, there is a large overlap between the bistable region of the system and positive feedback region of the PLS-PAI1 feedback loop (Figure 2.3D). KLF2 = 0 point lies in the overlapping area of the bistable region and PLS-PAI1 positive feedback region, while KLF2 = 100% lies in the overlapping area of the non-bistable region and PLS-PAI1 negative feedback region. This explains why the change of KLF2 level can have two different effects on the system.

The large overlap (Figure 2.3D) between the bistable region and the PLS-PAI1 positive feedback region is also an interesting property of the system, since it

suggests that in reality, a bistable TGF-β1 activation system most likely also has positive PLS-PAI1 feedback. Although a negative feedback loop between PLS-PAI1 has been observed repeatedly and is well accepted [48,49], positive feedback would be novel. We tested the sign of the feedback from PLS to PAI1 using an experimental system known to exhibit TGF-β1 bistability [1], a cell culture model of liver fibrosis. In this co-culture with primary hepatocytes and HSC-T6 cell lines, we added different levels of PLS and we measured PAI1 mRNA levels using RT-PCR (Figure 2.3B). Increasing PLS was found to cause decreased expression of PAI1 in this bistable system, implying that PLS and PAI1 can indeed exhibit positive feedback.

2.5 Discussion

We used computational modeling to explore the implications of a bistable TGF-β1 activation network, and we found (a) upstream factors like calcium and KLF2 could affect the steady state behavior of this bistable system, and (b) the steady state behavior of the system correlates with the sign of a feedback loop in the network.

For the first part, we modeled known effects of calcium on the balance between TSP1 and PLS [33,35,51-54], and known effects of KLF2 on the gene expression of PAI1 and TSP1 [37]. We then used modeling to show how these effects would propagate through the system. Specifically, the model predicted that calcium would significantly promote TGF-β1 activation,

shifting the bistable threshold of the system. The calcium-induced increase in TSP1 would lie within the physiological range of TSP1 [55]. A literature search reveals that extracellular calcium may be relatively easy to perturb via biomaterials of bandages. Therefore, the effect of extracellular calcium on TGF-β1 might have important therapeutic implications for fibrotic or inflammatory diseases where abnormal TGF-β1 contributes to disease. For example, fibrotic diseases are driven by high levels of TGF-β1 [56], and therapeutic studies in animals have achieved significant access by increasing the PLS pathway [57] or decreasing the TSP1 pathway [58]. In our model, if we take the ssP state to be healthy and the ssT state to be fibrotic, then a fibrotic system with high calcium could transition toward health through an increase of PLS (Figure 2.2C, arrow 1), through a decrease of TSP1 (Figure 2.2C, arrow 2), or a combination of both (Figure 2.2C, arrow 3).

In contrast, KLF2 was simulated to increase PLS activity and decrease the levels of TGF-β1, by suppressing PAI1 and TSP1 expression. This is consistent with previous work with statin drugs on liver fibrosis [36], where KLF2 upregulation was observed after treatment with simvastatin. Our model predicts that one of the ways KLF2 may contribute to improvement of liver fibrosis may be by decreasing the activation of TGF-β1 through reduction of the TSP1 and PAI feedback effects.

While modeling KLF2 effects, we noticed that loss of bistability also caused a

change in the sign of the PLS - PAI1 feedback loop. Without KLF2, the PLS-PAI1 feedback loop was positive (double negative), but with KLF2 (100% KLF2) and with the destruction of bistability, the PLS-PAI1 feedback loop was negative. Additional bifurcation analysis revealed that high KLF2 is a special case of the general observation, that the bistability of the system is correlated with the sign of the PLS-PAI1 feedback loop.

Finally, an *in vitro* experiment validated the positive feedback behavior between PLS and PAI1 in a bistable TGF-β1 system. Experiments have already seen two opposite behaviors of PLS towards TGF-β1 and PAI1 [48-50], providing indirect evidence for the possibility of both positive and negative feedback loops. Some aspects of the feedback loop are relatively unambiguous. For example, PAI1 is a specific and potent inhibitor of plasmin activation. PAI1 production follows TGF-β1 signaling so closely that, in practice, PAI1 levels are commonly measured as a readout of TGF-β1 activation [59]. The behavior of the feedback loop thus boils down to the behavior of the PLS – TGF-β1 relationship. In isolation, PLS clearly is able to activate TGF-β1. The same effect has frequently been observed in more physiological contexts, and there is considerable published evidence that PLS and/or plasminogen activators can cause an increase in TGF-β1 and/or PAI1 levels [43-47]. This positive effect of PLS on TGF-β1 or PAI1 serves as evidence that the loop between PLS and PAI1 can have negative feedback. Although the activating ability of PLS toward TGF-β1 is well known and

accepted, some studies also suggest the opposite effect. For example, PLS caused TGF-β2 levels to decline in breast cysts [60]. Furthermore, one unconventional finding by Seo et al., showed a positive feedback effect between PAI1 and TGF-β1 [50], suggesting that PLS can cause a decrease in TGF-β1. In sum, we conclude there is some support in the published literature for our prediction that the relationship between PLS and PAI can show either negative feedback or positive feedback, depending on context.

There are several caveats that should temper the interpretation of our modeling results. Firstly, the model used kinetics rate constants that were not known experimentally. Thus the behavior of the model should be taken as a qualitative prediction of trends rather than a quantitative prediction of absolute magnitude. Secondly, parameters taken from previous publications may be incorrect for our context, even if they were correct for the original context in which they were published. Thirdly, we have simplified complex processes into simplistic scalar variables. Even the effect of calcium on TSP1 has been greatly simplified, relative to the true effect, which is a change in the equilibrium between different conformations of TSP1. The simplified nature of our model implies that its predictions are low-resolution trends, not detailed molecular concentrations.

Another important consideration in interpreting this model is the redundancy of proteases and matrix factors that play roles similar to PLS or TSP1.

Actually, PLS is only one of many proteases (including elastase, MMP-2, MMP-9, ADAMTS1 and others) that can both activate TGF-β1 and cleave TSP1 [61-64]. Meanwhile TSP1 can inhibit many of these proteases [33,65-67]. Extracellular proteases often function interdependently by activating each other (e.g. PLS activates several MMPs, which activate other MMPs [68,69]), and some proteases may have partially redundant effects. Likewise TSP1 may represent a larger class of matrix proteins and mechanical factors with redundant roles in this model. Fibrillin and LTBP1 can promote TGF-β1 activation [70-73], as can factors that create mechanical tension in the matrix [74,75]. Fibrillin and LTBP1 can be cleaved by PLS [45,76], and even mechanical tension would be antagonized by PLS cleavage. In other words, PLS and TSP1 are archetypes of two larger classes of effects, a protease category and a matrix category, that may be capable of antagonizing the effect of each other, even as they contribute individually to TGF-β1 activation. The redundancy of the protease-versus-matrix competition suggests that this antagonism may be an organizing principle of TGF-β1 regulation, with evolutionary importance to the organism. On the other hand, this redundancy also creates many complexities that could perturb the phenomena we simulated. For example, the effects we attribute to PLS itself may actually result from the indirect effects of PLS-activated proteases. The low-resolution nature of our theoretical model necessitates a speculative outlook, but we believe it points to important considerations of system-level coordination.

2.6 Methods

2.6.1 TGF-β1 bistable activation model

We used the model built by Venkatraman *et al*. as the base model of TGF-β1 regulation. We increased the "k_{others}" parameter relative to the published model, to allow for higher basal activation of TGF-β1 by other activators such as integrins [18,70,77]. Simulations were performed using kroneckerbio toolbox [78] and the ode15s solver in MATLAB (Mathworks, Natick, MA).

2.6.2 Calcium model

Calcium can affect the structure of TSP1 [51-54], the enzymatic activity of PLS cleaving TSP1 [33], and the ability of TSP1 to inhibit serine protease activity [35]. These effects were represented by the rate constants k3, k_3 and k4 in the TGF-β1 activation model. We used the original parameter settings as the low calcium settings. To reflect high calcium conditions, we increased k3 by 10 fold, decreased k_3 by 0.1 fold, and k4 by 0.0001 fold, in order to reflect a high level of calcium in the environment. Details of the model can be found in Table 2.1 and Table 2.2.

Reaction equation	Reaction equation
$scUPA + PLG \xrightarrow{keff_1} PLS + scUPA$	$A2M + PLS \underset{k_{-5}}{\overset{k_5}{\rightleftarrows}} A2M : PLS$
$PLS + scUPA \xrightarrow{keff_2} tcUPA + PLS$	$PAI1 + tcUPA \underset{k_{-6}}{\overset{k_6}{\rightleftarrows}} PAI1 : tcUPA$
$tcUPA + PLG \xrightarrow{keff_3} PLS + tcUPA$	$PAI1 + scUPA \underset{k7}{\overset{k_7}{\rightleftarrows}} PAI1 : scUPA$
$PLS + LTGF\beta1 \xrightarrow{k_1} TGF\beta1 + PLS$	$PLS + scUPA \xrightarrow{keff_2} tcUPA + PLS$
$TSP1 + LTGF\beta1 \xrightarrow{k_2} TGF\beta1 + PLS$	$PLS + scUPA \xrightarrow{keff_2} tcUPA + PLS$
$LTGF\beta1 \xrightarrow{k_{others}} TGF\beta1$	$TSP1 : PLS \xrightarrow{k_8}$
$TGF\beta1 \xrightarrow{kp_1} TSP1$	$TGF\beta1 \xrightarrow{k_9}$
$TGF\beta1 \xrightarrow{kp_2} PAI1$	$\xrightarrow{\alpha_1} \{scUPA;\ LTGF\beta1;\ A2M\};\ \xrightarrow{\alpha_2} \{PLG\}$
$TSP1 + PLS \underset{k_{-3}}{\overset{k_3}{\rightleftarrows}} TSP1 : PLS$	$\{scUPA;\ LTGF\beta1;\ A2M\} \xrightarrow{\mu_{edeg}};$ $\{\text{all other protein species}\} \xrightarrow{\mu_{pdeg}}$
$TSP1 : PLS \xrightarrow{k_4} PLS$	

Table 2.1: List of equations and parameters used for model construction. Reactions of TGF-β1 activation model as described in [1]. Ordinary differential equations are generated from these equations using mass-action law.

Parameters	low calcium, [KLF2] = 0%	high calcium, [KLF2] = 0%	low calcium [KLF2] = 100%
$keff_1$	0.035 $\mu M^{-1}s^{-1}$	0.035 $\mu M^{-1}s^{-1}$	0.035 $\mu M^{-1}s^{-1}$
$keff_2$	0.35 $\mu M^{-1}s^{-1}$	0.35 $\mu M^{-1}s^{-1}$	0.35 $\mu M^{-1}s^{-1}$
$keff_3$	1.4 $\mu M^{-1}s^{-1}$	1.4 $\mu M^{-1}s^{-1}$	1.4 $\mu M^{-1}s^{-1}$
k_1	0.035 $\mu M^{-1}s^{-1}$	0.035 $\mu M^{-1}s^{-1}$	0.035 $\mu M^{-1}s^{-1}$
k_2	24.5 $\mu M^{-1}s^{-1}$	24.5 $\mu M^{-1}s^{-1}$	24.5 $\mu M^{-1}s^{-1}$
k_{others}	0.35 s^{-1}	0.35 s^{-1}	0.35 s^{-1}
kp_1	0.35 s^{-1}	0.35 s^{-1}	0.35/7.8 s^{-1}
kp_2	1.05 s^{-1}	1.05 s^{-1}	1.05/7.4 s^{-1}
k_3	17.5 $\mu M^{-1}s^{-1}$	175 $\mu M^{-1}s^{-1}$	17.5 $\mu M^{-1}s^{-1}$
k_{-3}	0.0245 s^{-1}	0.00245 s^{-1}	0.0245 s^{-1}
k_4	0.35 $\mu M^{-1}s^{-1}$	3.5×10^{-5} $\mu M^{-1}s^{-1}$	0.35 $\mu M^{-1}s^{-1}$
k_5	24.5 $\mu M^{-1}s^{-1}$	24.5 $\mu M^{-1}s^{-1}$	24.5 $\mu M^{-1}s^{-1}$
k_{-5}	0.0105 s^{-1}	0.0105 s^{-1}	0.0105 s^{-1}
k_6	0.035 $\mu M^{-1}s^{-1}$	0.035 $\mu M^{-1}s^{-1}$	0.035 $\mu M^{-1}s^{-1}$
k_{-6}	0.0035 s^{-1}	0.0035 s^{-1}	0.0035 s^{-1}
k_7	0.07 $\mu M^{-1}s^{-1}$	0.07 $\mu M^{-1}s^{-1}$	0.07 $\mu M^{-1}s^{-1}$
k_{-7}	0.0035 s^{-1}	0.0035 s^{-1}	0.0035 s^{-1}
k_8	24.5 s^{-1}	24.5 s^{-1}	24.5 s^{-1}
k_9	0.21 s^{-1}	0.21 s^{-1}	0.21 s^{-1}
μ_{edeg}	0.0525 s^{-1}	0.0525 s^{-1}	0.0525 s^{-1}
μ_{pdeg}	0.0175 s^{-1}	0.0175 s^{-1}	0.0175 s^{-1}
α_1	0.0035 s^{-1}	0.0035 s^{-1}	0.0035 s^{-1}
α_2	0.035 s^{-1}	0.035 s^{-1}	0.035 s^{-1}

Table 2.2: Parameters settings for different models. Reaction rates for TGF-β1 activation model. Parameters in the second column are the same as described in [1]. Red colored parameters are modified parameters to reflect the calcium effects. Blue colored parameters are modified parameters to reflect the KLF2 effects (kp1 reduced by 7.8 fold, kp2 reduced by 7.4 fold).

2.6.3 KLF2 model

It has been shown that KLF2 can decrease TSP1 expression by 7.8 fold and PAI1 expression by 7.4 fold [37,38]. We simulated the TGF-β1 activation model with no change (0% of the KLF2 effect, original parameter settings),

with 100% of the KLF2 effect (7.4 fold decrease of PAI1 synthesis parameter *kp2* and 7.8 fold decrease of TSP1 synthesis parameter *kp1*), as well as a series of intermediate models with 10%, 20%, … 90% of the KLF2 effect, causing intermediate levels of decrease in the PAI1 and TSP1 synthesis rates.

2.6.4 Bifurcation analysis

Bifurcation analysis was performed using MATCONT (http:// www.matcont.ugent.be). Equilibrium continuation function was called to generate the bifurcation curves in Figure 2.2E and Figure 2.3B.

2.6.5 Experimental methods

Isolation of primary hepatocytes was performed on male Wistar rats (250-300g), via a two-step collagenase perfusion method as described previously [79]. A co-culture model of primary rat hepatocytes and hepatic stellate cell line T6 (HSC-T6) was established as described in [1]. Briefly, primary rat hepatocytes were first seeded at a density of 2 x 10^5 cells on 35 mm collagen-coated dishes (IWAKI) using Williams's E media with 10% FBS. After 4 hours, hepatic stellate cell line T6 (HSC-T6) was seeded at a density of 1.4 x 10^6 cells. The cells were cultured overnight in 35°C, and 5% CO_2 in William's E media with 2% FBS to facilitate HSC activation. The next day media was changed to Williams's E without serum, along with different doses of PLS. After 24 hours, the cells were collected.

RT-PCR was performed as described in [2]. Briefly, mRNA was isolated from the cells using RNeasy mini kit (Qiagen), and its concentration was quantified using a Nanodrop 2000 UV-Vis Spectrophotometer. One microgram of mRNA from each sample was converted to cDNA (Invitrogen, Superscript Reverse Transcriptase III) and real-time PCR reaction (Roche, Sybr Green Master mix) was carried out for plasminogen activator inhibitor-1 (PAI1) and β-actin, with in-house primers shown in Table 2.3. The gene expression values were determined by the Del-Del C_T relative quantitation method; the target C_T values were normalized to the endogeneous reference β-actin, and the normalized mRNA was expressed as a fold-change relative to the untreated control.

Gene name	Primer sequences (5'-3')
β-actin	
Sense	ACCCACACTGTGCCCATCTA
Antisense	GCCACAGGATTCCATACCCA
PAI1	
Sense	TGGTGAACGCCCTCTATTTC
Antisense	GAGGGGCACATCTTTTTCAA

Table 2.3: List of primer sequences for genes probed on quantitative real time PCR.

2.6.6 Ethics statement

The rat cell isolation procedure was approved by the IACUC of National University of Singapore.

2.7 Conclusions

By integrating information from different modeling and literature sources, we predicted systems-level regulatory mechanisms and identified correlations between different qualitative behaviors. Specifically, our modeling illustrated how the balance between upstream factors could influence a bistable TGF-β activation system, and demonstrated a correlation between the bistability of the system and the sign of the feedback loop.

CHAPTER 3: THE RELATIVE ROBUSTNESS OF COMBINATION THERAPY IS CORRELATED WITH THE SYNERGY, FOR TRIGGERING SWITCHES OF BISTABLE SYSTEMS

3.1 Overview

This chapter focuses on the problem of combination targeting of the TGF-β1 bistable model. We will develop computational methods to study the combination targeting problem, and to estimate the level of synergy through simulation. We will study how parameter variations would affect the combination targeting. We will also see how analysis of the TGF-β1 bistable model led us to some general properties of many other bistable network models.

3.2 Abstract

Computational modeling of biochemical networks can be particularly useful for predicting which pairs of drugs will have synergistic versus additive effects. However, the success of prediction can be threatened by model uncertainty and parameter uncertainty. Additional challenges arise when models are bistable, due to the binary nature of the output. Bistability is an important aspect of biological regulation and it presents unique opportunities for therapeutic intervention, but little is known about the fragility of therapeutic predictions in such systems.

Using a model of bistable TGF-β1 activation, we perturbed individual and pairwise species to survey the additive and synergistic combinations. When model parameters were varied, we observed a biased pattern of change in the additive and synergistic curves for combination treatments. Parameter perturbation analysis revealed positive correlation between synergism and relative robustness throughout the TGF-β1 activation network. Correlation between synergism and relative robustness was also seen when repeating the perturbation analysis on multiple bistable models from different areas of biology.

A positive correlation between the synergy of a combination therapy, and the relative robustness of the combination doses, could be a general property of many bistable networks.

3.3 Background

Bistability is the ability of a system to converge to either of two stable steady states [5,80]. Bistability produces important biological behaviors such as allowing diverse inputs to converge toward a single binary (yes/no) decision, "remembering" a previously chosen steady state over time, remaining at the same steady state in the presence of random noise [81,82] and switching between two states with ultrasensitive response to a particular stimulus [83]. Some biological effects are binary at the level of single cells but graded-response for a population of cells [83], and some bistable effects

have binary output even for a population of cells [1]. A binary output presents novel challenges for drug design or target identification, because many design approaches rely on a graded dose-response curve.

Bistable network models have been built to study cell cycle progression [84], apoptosis [85-87], memory and plasticity control in cell differentiation [88,89], and enzyme activation networks [90,91]. For example in apoptosis, bistability enables many influences of cell stress and survival to induce a single decision whether to digest the cell's DNA and undergo apoptosis [85-87]. Bistability can also arise from genetic circuits. For example, a synthetic genetic network has been built in E. coli, showing bistability of a mutually inhibitory network composed of two repressible promoters [92]. Many previous studies of biological network bistability have characterized the determinants of bistability or the conditions that cause bistability to break down. In these studies, bifurcation analysis is often used to identify the boundaries of parameters that allow bistability of a network. Previous work has also focused on input-output models where an input stimulus triggers a bistable switch in an output. However, few bistable modeling projects have emphasized questions of drug targeting or therapeutic dosing.

Bistable systems may be particularly attractive to target with therapeutic interventions because they might permit a short-term treatment to cause a long-term switching effect. In a monostable system, drugs must be provided

continually to have a sustained effect; but in a bistable system, a compound could cause a switch to a stable steady state. In that case, endogenous network effects could maintain the system in the new steady state over time, even if the drug is withdrawn.

The use of computational models during drug targeting allows for efficient exploration of combination therapies and identification of synergistic combinations. Synergistic drugs provide greater efficacy than the individual component drugs, and there has been great interest in synergistic drugs because they can amplify efficacy without necessarily amplifying toxicity and side-effects [93-95]. A more precise formalization of synergism is quantified using the combination index (CI) [96]. Drugs with additive effect have CI = 1 and synergistic combinations have CI < 1 (Figure 3.S1A). To the best of our knowledge, previous studies of combination treatments have studied graded responses and continuous outputs, rather than bistable systems with discrete outputs. For example, in [95,97], the synergy is evaluated by the temporal profile of an output node in the network. In [98], Loewe additivity isobologram analysis was used to evaluate combination effects.

A significant challenge for computational modeling in drug target identification is due to the uncertainty of parameters in the model. Many of the qualitative relationships (e.g., Mek activates Erk) are well established, but the quantitative rate parameters are often unknown, even for a single cell line,

and certainly unknown for a population of patients. Modest differences in model parameters or expression levels can sometimes cause dramatic changes in behavior. In a network model, the required dose of a drug/perturbation to achieve the desired therapeutic intervention can be strongly dependent on variation in the model parameters. Robustness of a biological system is the ability to maintain its function in the presence of noise and fluctuation. We apply the concept of robustness to the drug design problem as follows: a robust therapy can achieve functional goals even when the targeted pathway exhibits patient diversity or uncertain parameters. Therapies with low robustness may be undesirable since the system has a higher chance of over-reacting or under-reacting when there is change in parameters.

In this work, we study how bistable systems respond to combination perturbations, with or without parameter variation. First, we study the transition between two steady states induced by perturbing one or more nodes of a bistable system. We use a model of bistable TGF-β1 activation [1] as a case study for the effects of combination perturbations in a bistable system. Single species perturbation analysis computes the minimum threshold perturbation (critical dose) that can induce state switch, and also gives a list of species/nodes that have infinite critical doses (unable to switch the system). Combination perturbation analysis evaluates the effects of different combination pairs, to see which are additive or synergistic. Using the results from large-scale repetition of the perturbation analysis, we discovered a trend

in the robustness of combination drug doses. Under parameter perturbation, even when there was a dramatic change in the critical doses for single-species perturbations, synergistic combinations showed little change in critical dose. In other words, for synergistic pairs, the combination doses have higher relative robustness under parameter perturbation, than additive or antagonistic pairs. The correlation between robustness and synergy was very intriguing and we asked whether it was specific to the TGF-β1 system. We tested a range of previously published bistable models including cell differentiation [88,89], apoptosis [85], cell cycle entry [84], and robust motifs of bistability [99]. In every case, we found a correlation between dose robustness and synergy, suggesting that the correlation between robustness and synergy is a general property of many bistable networks. Our result suggests that perturbations (i.e., drug therapies) to modify a bistable system will have more robust functional effects if the perturbations target synergistic nodes of the network. Finally we discuss the implications for targeting and dosing in drug design.

3.4 Results

3.4.1 Single species and combination species perturbation of a bistable TGF-β1 activation network

For comparing the effects of single perturbations and combination perturbations on the steady states of a bistable system, we needed a mid-sized model of a bistable biochemical network. We selected our previously

published model of TGF-β1 activation by Thrombospondin (TSP) and plasmin (PLS) [1]. In this model, TGF-β1 had a positive feedback loop with one activator, TSP, and a negative feedback loop with the other activator, PLS. Because TSP and PLS were mutually antagonistic, this system showed bistable behavior, with one steady state having high levels of TGF-β1 (activated primarily by TSP while PLS was off) and one steady state having lower levels of TGF-β1 (activated predominantly by PLS, while TSP was off). These two steady states showed a qualitative resemblance to normal and fibrotic modes of behavior in liver cells. A simplified reaction diagram appears in Figure 3.1A.

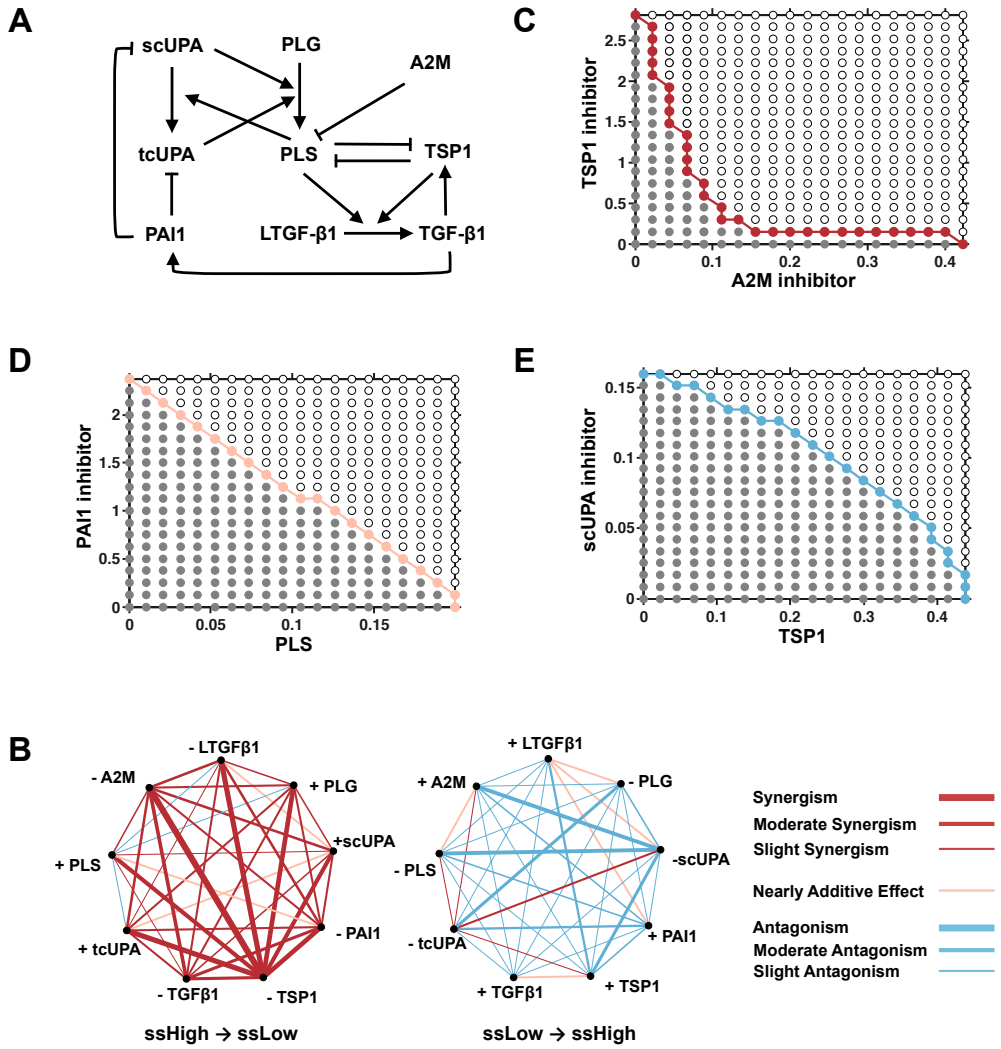

Figure 3.1: Combination species perturbation of a bistable TGF-β1 activation model. (A) Reaction diagram of the TGF-β1 activation network. Arrow means "activates" or "enhance". Arrow with bar end means "inhibits". (B) Polygonogram [100] of the combination index (CI) for all pairs of species in the target lists capable of switching the system from ssHigh to ssLow (left) and from ssLow to ssHigh (right). A negative sign (-) indicates a negative perturbation of the species (i.e., adding inhibitors), and a positive sign (+) indicates a positive perturbation of species (i.e., adding more of the species). There are 36 possible combinations for each polygonogram. Synergistic combinations are represented by red lines. Nearly additive combinations are represented by light pink lines. Antagonist combinations are represented by cyan lines. The level of synergism and antagonism are reflected from the thickness of the lines. (C) A combination diagram showing system convergence to ssHigh or ssLow for different combined doses of TSP1 inhibitor and A2M inhibitor. (D) A combination diagram showing system convergence to ssHigh or ssLow for different combined doses of PAI1

inhibitor and PLS. (E) A combination diagram showing system convergence to ssLow or ssHigh for different combined doses of scUPA inhibitor and TSP1. In (C) and (D), the system was initialized to ssHigh and so convergence to ssHigh means failure to switch the steady state, while convergence to ssLow means succeeding to switch the steady state. In (E), the system was initialized to ssLow and so convergence to ssLow means failture to switch the steady state, while convergence to sHigh means being able to switch the steady state. In (C)-(E), gray dots represent dose combinations that fail to switch steady states, and black circles represent dose combinations that are able to switch steady states. In (C)-(E), the separatrix (boundary between gray dots and black circles) are highlighted with red, pink and cyan colors for synergism, additivity and antagonism respectively.

We used this model to study combinations of anti-TGF-β1 and pro-TGF-β1 perturbations. To identify potential targets for switching the steady state of the system, we performed single species perturbation analysis. Briefly, for anti-TGF-β1 perturbations, we initialized the system in the steady state with high TGF-β1 (SShigh), then every species in the system was perturbed up or down individually, to test whether the system would re-converge to the SShigh state, or converge instead to the steady state with low TGF-β1 (SSlow). Table 3.S1C shows the minimum perturbation magnitude (the critical dose) for each species to switch the bistable TGF-β1 network from SShigh to SSlow. For pro-TGF-β1 perturbation, the system was initialized with SSlow instead.

Based on the critical doses obtained from single species perturbation analysis, we performed combination species perturbation analysis (Figure 3.1B-E). Full details of all perturbation studies appear under Methods. Briefly, we discretized the intervals from zero to the estimated critical doses of each perturbation, and applied the combination of each pair of doses to the system

in SShigh (or SSlow) and simulate the effect. If a dose combination was able to switch the system to SSlow (or SShigh), we plotted a black circle at the dose combination point, if not, we plotted a gray dot (Figure 3.1C-E). In this plot, which we call a "combination diagram", the boundary (separatrix) between the switch and non-switch regions represents the "**critical combination doses**" for switching the steady state of the system. The separatrix is analogous to the ED50 isobologram in the evaluation of combination therapy, therefore we apply the Combination Index (CI) [96] method to evaluate the combination effect for the dose combinations on the separatrix (Figure 3.S1A-B). A representative CI (See Methods) is selected for each pair of target combination, and is plotted on a polygonogram [100] (Figure 3.1B).

Figure 3.1C shows the combination diagram of a synergistic combination with anti-TGF-β1, TSP1 inhibitor with A2M inhibitor. The shape of the synergistic separatrix is bending towards the origin. Figure 3.1D shows the combination diagram of an additive combination with anti-TGF-β1 effect, PLS and PAI1 inhibitor, in which the separatrix is a straight line. Figure 3.1E shows the combination diagram of an antagonistic combination with pro-TGF-β1 effect, TSP1 and scUPA inhibitor, in which the separatrix is bending outward. The method to estimate separatrix by numerical simulation is provided in Methods Section 4.

3.4.2 Parameter perturbation analysis of combination species perturbation of TGF-β1 activation network

We started our analysis by using the published parameters of the model, but since many of the parameters were uncertain or estimated, we performed parameter perturbation analysis (see Methods) to test the robustness of each synergistic combination to parameter variation. Interestingly, we found that the critical combination doses of the synergistic combinations varied in a much less sensitive manner (Figure 3.2A) than the individual critical doses of each of each components of the combination (for the same amount of parameter perturbation). In contrast, for additive combinations, the critical combination doses varied in parallel with the critical doses of the components (Figure 3.2B), and for antagonistic combinations, the critical combination doses varied in an even more sensitive manner than the critical doses of the components (Figure 3.2C).

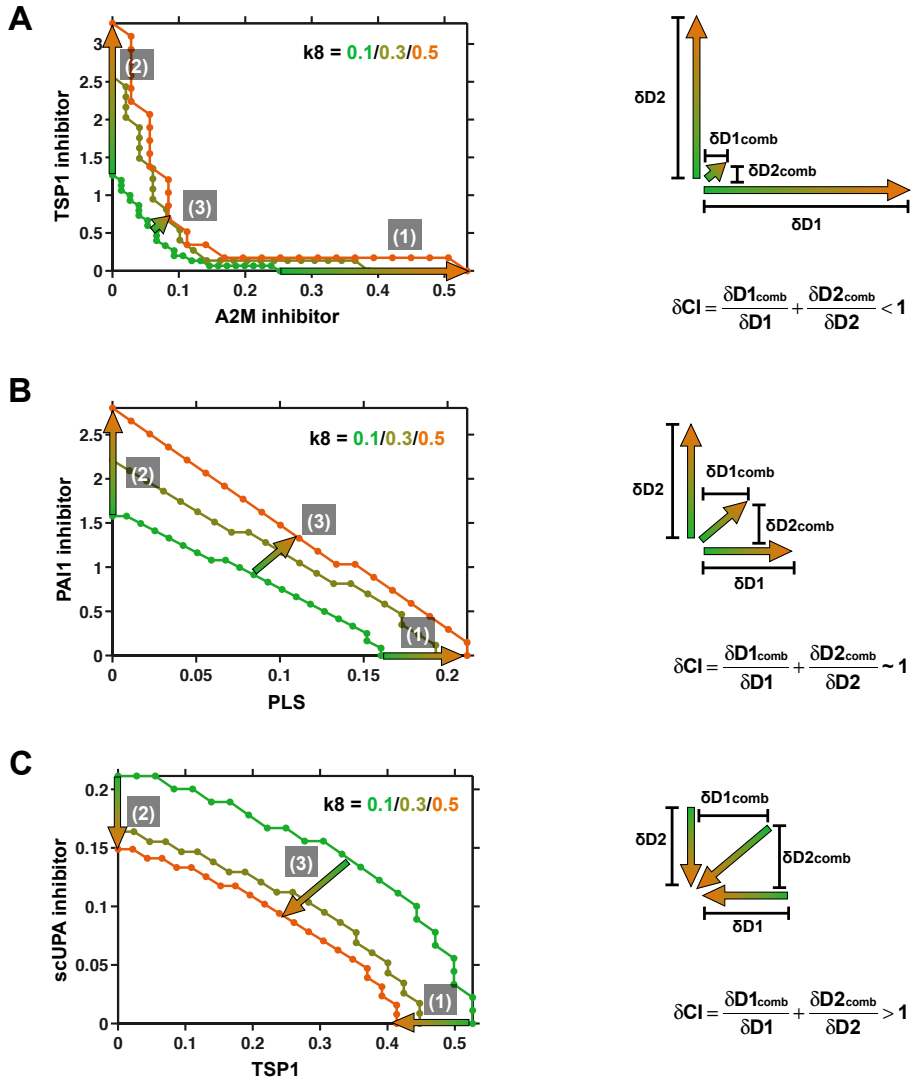

Figure 3.2: Different responses of synergistic and additive combinations to parameter variation. Shifts in the separatrix when the system has three different values for parameter k_8 (called k_{others} in [1]). The green separatrix represents the system with $k_8 = 0.1$. The brown dotted separatrix represents $k_8 = 0.3$, and the orange dotted separatrix represents $k_8 = 0.5$. Arrow 1 (with length δD1) depicts the change of critical dose for the first species in the combination, when k_8 is increased from 0.1 to 0.5. Arrow 2 (with length δD2) depicts the change of critical dose of second species in the combination, when k_8 is increased from 0.1 to 0.5. Arrow 3 (with horizontal length $\delta D1_{comb}$ and vertical length $\delta D2_{comb}$) depicts the change in the representative dose combination (See Methods). (A) The shift in separatrix for a synergistic combination (negative perturbation of TSP1 and negative perturbation of A2M). (B) The shift in separatrix for an additive combination (positive perturbation of PLS and negative perturbation of PAI1, plasminogen activator

inhibitor-1). (C) The shift in inparatrix for an antagonistic combination (negative perturbation of scUPA and positive perturbation of TSP1).

Figure 3.2A-C shows the change of critical combination doses (i.e., the change in separatrix) for the combination diagrams of a synergistic pair ("-TSP1, -A2M"), an additive pair ("-PAI1, +PLS") and an antagonistic pair ("-scUPA, +TSP1") when we vary one parameter "k_8". k_8 (called k_others in the previous publication) was chosen first because we believed k_8 is particularly likely to vary with the context. k_8 describes the activation of TGF-β1 by "other" activators not explicitly included in the model. We set 3 values for "k_8", i.e. 0.1, 0.3, and 0.5 (Figure 3.2A-C) The green, dark green, orange color in Figure 3.2A-B represent the critical combination doses (i.e., the separatrix) when "k_8" equals 0.1, 0.3, 0.5, respectively. We observed that for combination perturbation with strong synergy (Figure 3.2A), comparing with the dramatic change of critical dose of each of its components (Figure 3.2A, arrow 1 and 2), the combination doses just change a small amount (Figure 3.2A arrow 3). For additive combinations, the combination dose change (Figure 3.2B, arrow 3) is approximately the linear combination of single component dose change (Figure 3.2B arrow 1 and 2). While for antagonistic combinations, the combination dose change is even more than additive combinations (Figure 3.2C).

To quantify how the separatrix and the critical dose combinations would change in response to perturbation of individual parameters, we used the

relative robustness (RR) method. The variables are depicted graphically in Figure 3.2 and defined in the following formula (see Methods for details).

$$\Delta CI = \frac{\delta D1\_comb}{\delta D1} + \frac{\delta D2\_comb}{\delta D2};$$

$$RR = 1 - \Delta CI;$$

ΔCI measures the relative advantage of combination perturbation over single component perturbation of either of its components, in terms of dose variation due to parameter uncertainty. A combination with a small ΔCI can have more robust critical combination doses than a combination with large ΔCI if the robustness of the critical doses of their components are on similar levels. We therefore defined relative robustness to be the inverse of the ΔCI, i.e. RR = 1-ΔCI.

3.4.3 Relative dose robustness is positively correlated with synergy in the model of bistable TGF-β1 activation

The stark difference in RR of the synergistic combination ("TSP1 and -A2M"), the additive combination ("-PAI1 and PLS") and antagonistic combination ("-scUPA, +TSP1") in Fig2, and similar trend we observed from other pairs of species under different parameter perturbations (Figure 3.S2A-D) motivated us to compute the RR of other synergistic combinations due to perturbation of other parameters, and compare against the RR of other additive combinations, in the same TGF-β1 model. All 36 pairs of perturbations for

switching the TGF-β1 system from SShigh to SSlow were considered (Table 3.S1D). In addition to repeating the single parameter perturbation method (Figure 3.3A,C), we also performed multiple parameter perturbation (Figure 3.3B,D). We used the mean CI value between the unperturbed system and the perturbed system (CI_{mid}, see equation (5) in Methods) to represent the synergy level of a species combination. In Figure 3.3A-B, the RR and C_{mid} distributions are shown as box plots for each of the 36 pairs of species. Regardless of how the parameters were perturbed, we observed a negative correlation between the RR and CI_{mid} distributions, which was quantified by plotting the mean RR versus the mean CI_{mid} for each of the 36 pairs (Figure 3.3C-D).

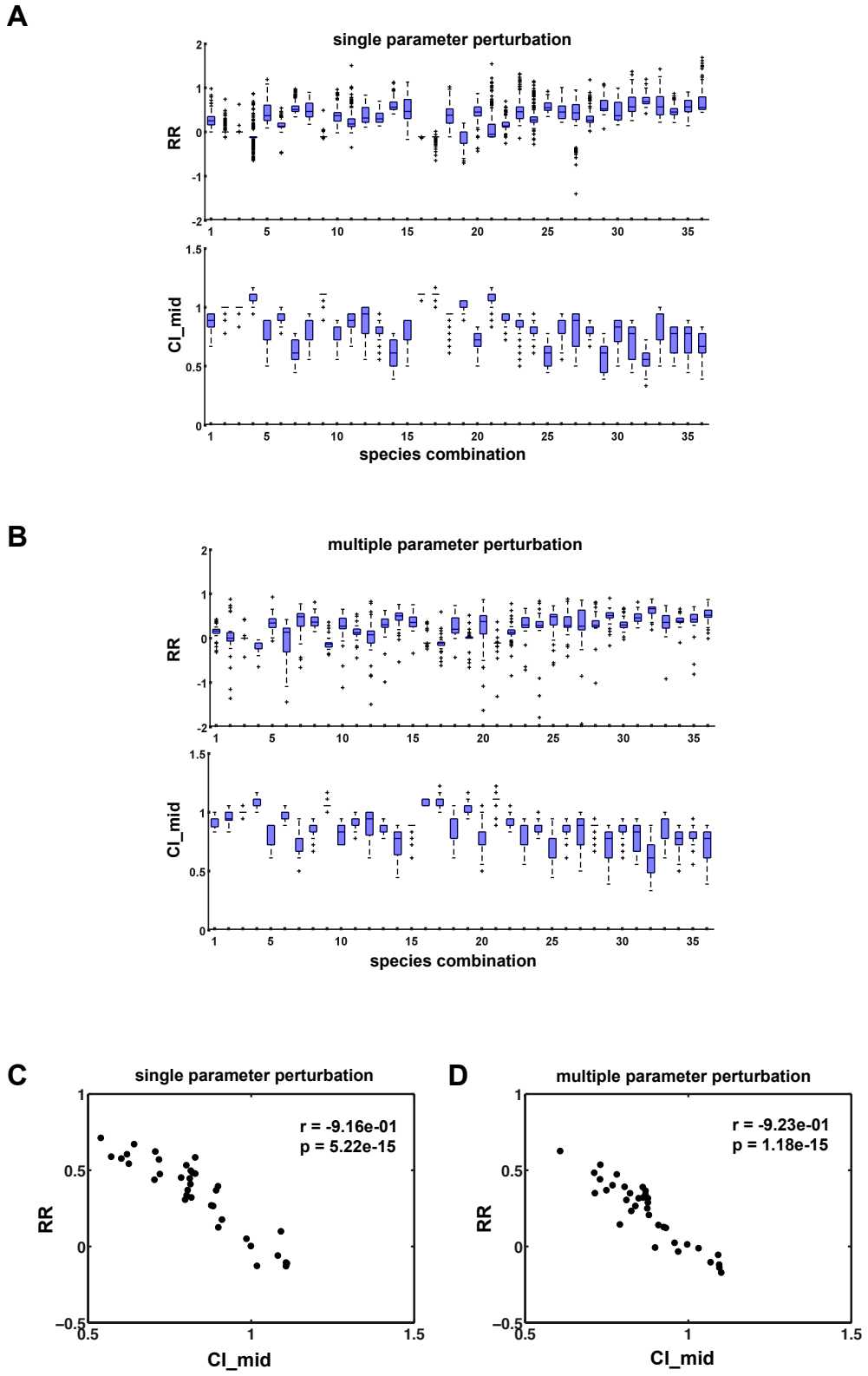

Figure 3.3: Parameter perturbation analysis to evaluate relative robustness (RR) and synergy for all anti-TGFβ1-activation combinations. (A-B) For the 36 possible combinations of species (x-axis), box plots show the

relative robustness of the combination critical dose and the CI_{mid} combination index, computed by (A) single parameter or (B) multiple parameter perturbation analysis. (C-D) A scatterplot of the mean CI_{mid}, versus the mean RR, for each species combination, resulting from (C) single parameter or (D) multiple parameter perturbation analysis.

Through parameter perturbation analysis, we confirmed that the relative robustness (RR) of **critical combination doses** is indeed positively correlated with synergy (negatively correlated with CI_{mid}), for switching the TGF-β1 activation system from SShigh to SSlow (i.e., anti-TGF-β1 therapies).

We repeated the entire procedure for the opposite switch of the same system (i.e., pro-TGF-β1 therapies). We considered all possible combination perturbations for switching the TGF-β1 steady state from SSlow to SShigh. An opposite switch of the same system is not expected to give the same trends because if one method (e.g. –TSP1 and –A2M) is relatively easy or synergistic to perturb the system in one direction, its opposite method (e.g. TSP1 and A2M) might be relatively hard or antagonistic to perturb the system in the other direction. With such intuition, we think it is necessary to study both directions of the switch to check whether the correlation between RR and CI is direction relevant. Figure 3.4A shows the species combinations for two directions of switching for the TGF-β1 bistable model. The blue dots represent anti-TGF-β1 activation combinations while the red dots represent pro-TGF-β1 activation combinations. We observed that the anti-TGF-β1 treatments were synergistic on average, while the pro-TGF-β1 treatments were antagonistic on

average. Nonetheless, the correlation between RR and CI followed the same trend.

3.4.4 The correlation between relative robustness and synergy is a general property of many bistable biological networks.

To test the generality of the correlation between RR and CI, we analyzed several additional bistable networks. The entire multiple parameter perturbation analysis was repeated for bistable biological network models of apoptosis (Figure 3.4B), hematopoietic cell fate (Figure 3.4C), the ETT regulatory motif (Figure 3.4D), cell cycle entry (Supplementary Figure 3.S3A), and cell differentiation (Supplementary Figure 3.S3B). The details of the steady states, parameter settings, critical doses and species combinations of the models can be found in Supplementary Tables 3.S1-6. A significant positive correlation between RR and synergy (a negative correlation between RR and CI) was observed for all bistable systems tested. We conclude that bistable models often display a significant positive correlation between synergy and relative robustness, under parameter uncertainty.

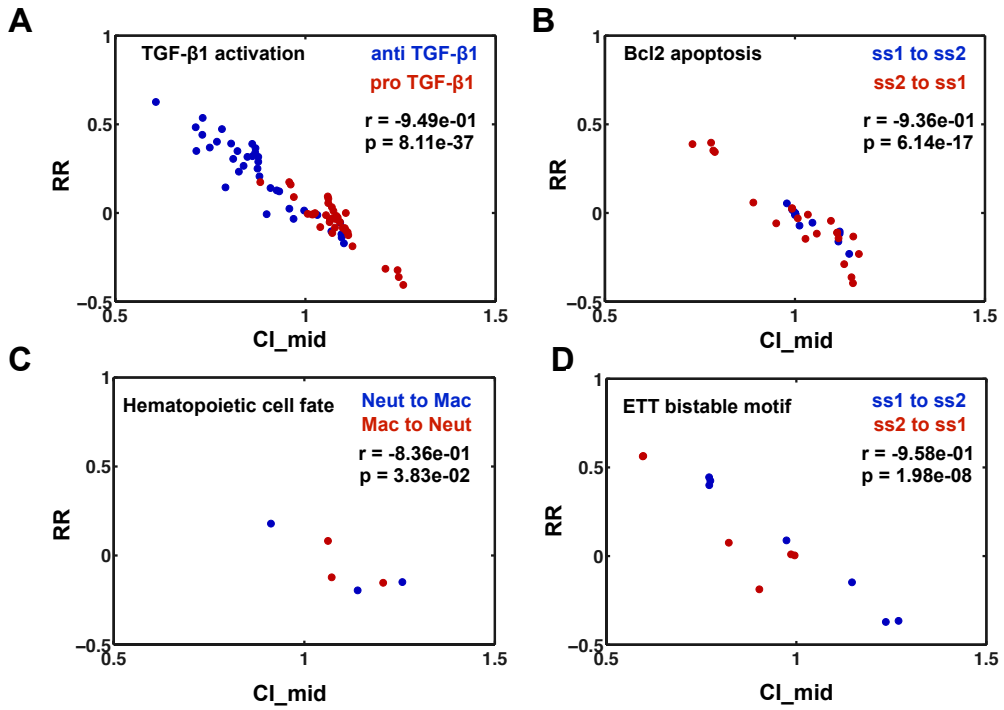

Figure 3.4: Multiple parameter perturbation analysis of bistable models of different biological systems. A list of positive and negative species perturbations, capable of switching the system from either direction was generated through single species perturbation analysis (see Methods). For each pair of species, multiple parameter perturbation analysis was performed, which yields mean C_{mid} (see Methods) and mean RR. The RR v.s. CI_{mid} for each pair of species was shown in a scatter plot. (A) TGF-β1 activation model with both directions of switch considered [1]. (B) Bcl2 apoptosis model [85]. (C) Hematopoietic cell fate model [89]. (D) EET bistable motif [99]. Additional cases are shown in Supplementary Figure 3.S3.

3.5 Discussion

Network models have played an increasing role in drug target selection, but bistable models have rarely been used for target selection. Drug development efforts sometimes need to target biological phenomena that are inherently bistable (e.g., apoptosis). At the same time, a growing number of biological events have been understood to possess bistability [84-88,90,91],

accompanied by a growth in the number of bistable network models. It is therefore timely to explore drug targeting in computational models of bistable systems. In this work, we used a TGF-β1 bistable activation model to study the problem of combination targeting of bistable systems. As expected, we found that different target combinations yielded different levels of synergism. More interestingly, we found that the synergism of a combination was related to the robustness. To be precise, when model parameters underwent modest fluctuations (within the bistable regime of the system), the relative robustness of the combination doses was positively correlated with the combination index. The parameter fluctuations were performed by applying single-parameter and multiple-parameter perturbation method. The relative robustness was defined by the sum of relative changes of combination doses over single doses as defined by equations (3)-(4) in the Methods section, and the synergy was defined by the combination index (CI) methods. After repeating the same analysis on several other bistable network models, all cases exhibited some degree of positive correlation between RR (relative robustness) and synergy (negative correlation between RR and CI). This suggests that a correlation between robustness and synergism may be a general property of combination dosing for many bistable network models.

We used RR (relative robustness) to characterize the dose variation of combination perturbation, for different levels of synergy. RR (a derivative of ΔCI) is a geometrical measurement of the change of separatrix in its shape and

position in combination diagram (Figure 3.5). Figure 5 lists several geometrically possible patterns of separatrix change when there is parameter perturbation. Our study identified that, in bistable systems two patterns (Figure 3.5 first row) are preferred for synergistic combinations and antagonistic combinations respectively, which reflect a positive correlation between RR and synergy. The correlation between RR and synergy can be understood by considering a Boolean simplification of the distinction between additive and synergistic pairs. With an additive pair, either species is capable of causing the downstream effect, and any amount of one species can be substituted by the other species. The switch depends on whether there is enough of species A OR species B, so an additive combination is like an OR operation. With a synergistic pair, the combination of both species is highly effective at causing the switch, but either single species alone is much less effective. The switch depends on the co-existence of species A AND species B. The RR (relative robustness) of switches caused by additive pairs is moderate because the switch depends on the doses of the two triggers, and any perturbation in the effectiveness of one species will have a linear effect on the necessary compensatory dose for the other species. The RR (relative robustness) of synergistic pairs is better because the switch depends strongly on whether A and B are both present, and weakly on the exact amount of each component. A perturbation of the effectiveness of one species will have less than linear effect on the necessary compensatory dose of the other species, provided neither species is near zero, meaning the combination remains near

the elbow of the curve in Figure 3.2A. It is worthwhile to note that the positive correlation between RR and synergy is not equivalent to the positive correlation between the robustness of critical combination doses and synergy, due to the fact that RR is a measurement of relative dose-variation. Two extreme cases (Figure 3.S4) demonstrate that in practice, dose robustness could be roughly the same (Figure 3.S4A) or dramatically different (Figure 3.S4B) for synergistic and antagonistic combinations. Figure 3.S4 also shows that information of the dose robustness of individual components, and their absolute dose value would be useful in evaluating the robustness of combination doses.

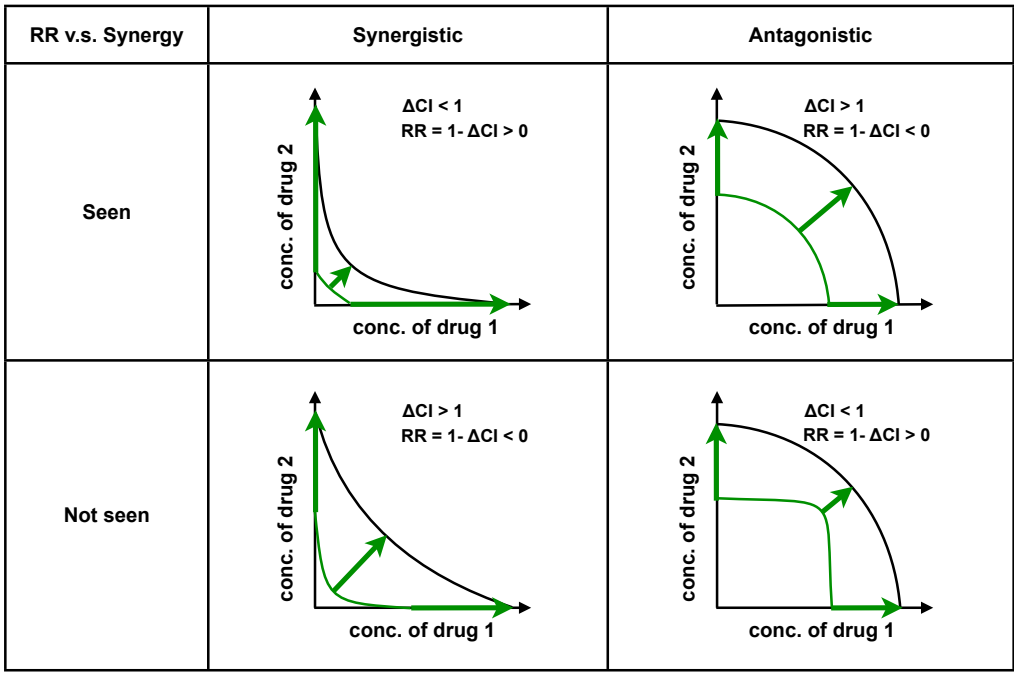

Figure 3.5: Preferred and non-preferred separatrix shift in bistable systems. Geometrically possible shift of separatrix for synergistic combinations and antagonistic combinations. Green and black curves represent the separatrix of two conditions of a bistable biological system

differing their parameters. Green arrows depict the change in critical doses of each component, and critical combination doses.

Uncertainty is a ubiquitous problem in network modeling of biological systems. Network models are composed of chemical reactions based on previous results from cell free assays or in vitro assays. Usually, most of the reaction rates have never been measured directly, and often they are estimated by fitting the global behavior of the system to observed dynamics [101], or by analogy with homologous systems. Even if reaction rates could be determined comprehensively and accurately, there will always be parameter uncertainty due to the differences between *in vitro* and *in vivo*, and due to patient-to-patient variation. The practical use of computational models can be facilitated by robustness analysis, even when the models have considerable uncertainty [102]. Robustness analysis quantifies how the model behavior changes in response to the uncertain variables, so the practical use of the model can be based on its robust behaviors (and conversely, so conclusions won't be drawn from its fragile behaviors). This traditional use of robustness analysis is complemented by our use of robustness analysis to study **dose robustness.** Dose robustness is the robustness of effective doses to change the state of the system when there is uncertainty/variation in the system parameters. Our discovery that the relative robustness of critical combination doses is negatively correlated with Combination Index (CI) (positively correlated with synergy) provides a prediction that administering a synergistic combination of treatments can be a choice to increase the dose robustness of the treatment.

Synergistic treatments are by definition able to achieve the same efficacy with lower doses (compared with non-synergistic combinations), and here we show that they also have the potential to achieve a narrower confidence interval on the therapeutic effect, in the presence of uncertainty.

One important application of computational network models is drug target identification and selection. Kitano proposed in 2007 to target the most sensitive ("fragile") nodes in a network, on the grounds that a small perturbation (a low dose of inhibitor) directed at a sensitive node would have greater impact (increased efficacy) [103]. Several subsequent studies have followed Kitano's strategy [104-108], but these studies have not addressed the impact of network uncertainty on the dosing uncertainty. Dose uncertainty is important in theory and in practice, because it increases the probability of under-dosing or over-dosing, when there is model uncertainty or patient variation. In this study we suggest a new targeting strategy that optimizes dose robustness by selecting synergistic target combinations. Under Kitano's strategy, the design goal was to minimize the absolute sum of the therapeutic doses, for a single, average-case model. In contrast, the design goal of our strategy is to maximize the dose robustness in the presence of parameter uncertainty (we use parameter uncertainty to represent both patient variation and model uncertainty). Kitano's goal of minimizing the absolute dose is mathematically optimal for minimizing toxicity in a single ideal model, and it leads logically to the strategy of targeting sensitive nodes. Our goal of

maximizing the dose robustness optimizes a different type of toxicity, which may be equally important in practice.

Because bistable systems have two stable steady states, the impact of a treatment is an all-or-nothing effect: either remaining in the current steady state or switching to the other steady state (for each tissue, each cell, or each unit of bistability). For systems with many small units, the dose response may be a sum of many binary effects, but if the system has a small number of large units, the dose response will have sharp cliffs, reflecting the success or failure to switch the states. A sharp dose-response curve is rare in drug development. Dose-response information is extremely valuable [109] and a gradual slope provides an intuitive way to adjust the response by adjusting the dose. A biological system with inherently sharp dose-response curves would violate the expectation of a tunable dose-response, and would be undesirable to target. In the long run, however, some biological systems may be unavoidably bistable, and some pathology may have inherent ultrasensitivity, regardless of how they are targeted. Our work, on combination targeting of bistable systems, contributes to a novel foundation for rational dosing, in systems where dose sensitivity dominates the risk profile.

The cliff-like separatrix of a bistable response creates an urgent motivation for seeking dosing strategies that are robust to parameter uncertainty, and hence we have explored the RR-synergy correlation first in bistable systems. The

RR-synergy correlation we found is not exclusive to bistable systems (data not shown), but we have focused on bistable systems because their steep dose-response behaviors motivate our emphasis on dose robustness. For future work, the prevalence of the RR-synergy correlation should be assessed in other regimes (e.g. monostable, oscillating.)

3.6 Methods

3.6.1 Definitions and the stable steady states.

Let d**x**/dt = **F**(**x**,**p0**) be a bistable model, where **p0** is the constant parameter vector, and **x** is the variable vector of biochemical concentrations. By the definition of bistability, there are two stable steady state values of **x**, which we call **ss1** and **ss2**. For most models, the **ss1** and **ss2** vectors were published, or easily derived from published information. For the ETT bistable models, bistability was studied over a range of parameters, but no specific value of the **p0** vector was published. Therefore, we performed repeated simulations with random initialization, to search for feasible values of **p0**, **ss1** and **ss2**.

3.6.2 Inhibitory species

Inhibitors of each species were added explicitly as new species into the model equations. For each species i, an irreversible (destructive) reaction between the i*th* species and its respective inhibitor was inserted using the

following mass-action chemical reaction: **x**(i) + **x_inhibitors**(i) → **x_inhibitor_complexes** (i). By definition the **x_inhibitor_complexes** species had no activity. The expanded model with inhibitory reactions can be written as $d\mathbf{x}_{long}/dt = \mathbf{F}_{long}(\mathbf{x}_{long}, \mathbf{p0}, \mathbf{k\_inhibitors})$, where $\mathbf{x}_{long}$ = **[x, x_inhibitors, x_inhibitor_complexes]**.

3.6.3 Single species perturbation analysis

For perturbation analysis of species i in the transition from **ss1** to **ss2** (or vice versa), the system was initialized with all species at the steady state level **ss1**, except with a perturbation of **x**(i) or **x_inhibitors**(i), prior to simulating the system trajectory. In other words, the perturbed initial condition, **x**(t = 0), was set equal to **ss1** + **δ_xi**, where **δ_xi** is a vector with all zeroes except a positive value for the **x**(i) or **x_inhibitors**(i) entry. Positive perturbations were performed by adding positive amounts δ to **x**(i). Negative perturbations were performed by adding positive amount δ, to **x_inhibitors**(i). The system was then simulated until steady state convergence. For each species i, the simulation was repeated many times with a series of positive or negative perturbations. A "dose response" curve was then plotted showing the final steady state of the system as a function of δ. Due to the stability property of the **ss1** steady state, the simulated trajectories would converge back to **ss1** if the perturbations were sufficiently small. As expected, the dose response plots did not show a change of steady state after small perturbations, and but many showed a jump to **ss2** for perturbations above some threshold. We call that

threshold perturbation the **critical dose**. The critical dose was estimated numerically for each species by the method of bisection. The above procedure was performed for each species i, and for each direction of the system transition, **ss1** to **ss2** and from **ss2** to **ss1**.

For each direction of the system transition, we compiled a **target list** of species, which were the species capable of switching the steady state, either as positive or negative perturbations. This list (and the respective critical doses) serve as input for combination species perturbation analysis and parameter perturbation analysis. Note that no more than one type of perturbation (either positive or negative) was found in our analysis to induce a switch from **ss1** to **ss2**. If a positive (or negative) perturbation of species i could induce a transition from **ss1** to **ss2**, then it was often (but not always) the case that an opposite-signed perturbation of species i could induce the opposite transition, from **ss2** to **ss1**.

3.6.4 Combination species perturbation analysis

Combination perturbation analysis resembled single species perturbation analysis, except perturbing two species or species inhibitors at the same time. Simultaneous perturbation of more than 2 species would be possible in theory, but were not considered in this study. Pairs of species (i,j) were taken from the list of species found to be capable of switching the system state during single species perturbation analysis. For each species, a set of N perturbation

magnitudes was selected, using equally spaced values between zero and the critical dose. N = 20 was used in Figure 3.1C-D, Figure 3.2A-B, while N = 10 was used for synergy and robustness estimation in Figure 3.3 and Figure 3.4. The bistable system was initialized N^2 times, such that all species were at their steady state levels except species i and j, which were perturbed by every pairwise combination of the chosen N perturbation amounts. Finally the N^2 initialized systems were simulated until convergence to a steady state. As with single-species perturbations, a "negative" perturbation of x(i) was performed through a positive perturbation of x-inhibitor(i).

A plot of the combination effects used color for indicating convergence to either **ss1** or **ss2**, for each pair of perturbation magnitudes. The plots of combination effects showed an obvious line or curve, called a **separatrix**, dividing the switch and non-switch regions of the plot. The separatrix was extracted for the quantification of synergy. The synergy was quantified using the combination index (CI) method as follows.

$$CI = \sum_{i=1}^{2} \frac{separatrix\_xi}{critical\_xi}; \qquad (1)$$

where critical_xi denotes the critical dose of species xi from single species perturbation analysis in the model; separatrix_xi denotes the combinatorial dose of xi on the separatrix in the combination plot.

We defined the **representative dose combination** depending on the synergy/ antagonism of the combination. For synergistic combinations, the

representative dose combination was the point on the separatrix with minimum CI (maximum synergy). For antagonistic combinations, the representative combination dose was the point on the separatrix with maximum CI (maximum antagonism). For additive combinations, it was the point on the separatrix with the most equal relative doses, meaning both species dosed at 50% of their respective critical doses. Therefore, we have:

$$CI\_rep = \sum_{i=1}^{2} \frac{rep\_xi}{critical\_xi}; \qquad (2)$$

We chose this definition of the representative dose combination because it provided continuity of doses (in the bistable models we studied) when parameter variation changed the shape and position of the separatrix.

3.6.5 Single parameter perturbation analysis

For each parameter **p0**(i), we used numerical simulation to find upward and downward perturbations that would disrupt the original bistability of the system, defined as the ability of the system to converge to two different steady states if initialized at **ss1** and **ss2**. The upward (or downward) perturbation was first estimated by repeated doubling (of halving) of the **p0**(i) value, until simulation of the system, initialized at **ss1** and **ss2**, failed to show convergence to two different steady states. Subsequent refinement of the upward and downward perturbations was achieved by bisecting the search interval until it was less than 1%. Finally the range between the upward and downward perturbation was discretized into N=20 equally spaced values, to provide a

range of values for **p0**(i). N systems were constructed, with each of the N values of parameter **p0**(i), and subjected to combination species perturbation analysis. In case a perturbed model became insensitive to a species in the target list (i.e., the species was no longer capable of causing a switch of the steady state), then that species was omitted from the combination species perturbation analysis.

The single parameter perturbation method was repeated for each parameter. Also for each parameter, the upward and downward perturbation range identified during single parameter perturbation was provided as input for the method of multiple parameter perturbation.

3.6.6 Multiple parameter perturbation analysis

All parameters were varied randomly and simultaneously, within their respective ranges. If we had sampled this high-dimensional parameter space with a uniform distribution, only a small fraction of the resulting systems would have shown bistability. We therefore sampled the parameter space using a beta distribution in each dimension, with mean at the unperturbed value and boundaries defined by the perturbation range. The probability of selecting a value for parameter p(i) was:

$$\Pr(\mathbf{p}(i)) = \text{Beta}(\alpha(i), \beta(i)) \times (\mathbf{p}_{\text{upper}}(i) - \mathbf{p}_{\text{lower}}(i)) + \mathbf{p}_{\text{lower}}(i)$$

where:

$$\alpha(i) = \frac{\mathbf{p}0(i) - \mathbf{p}_{\mathbf{lower}}(i)}{\mathbf{p}_{\mathbf{upper}}(i) - \mathbf{p}_{\mathbf{lower}}(i)} \times N_{beta}$$

$$\alpha(i) = \frac{\mathbf{p}_{\mathbf{upper}}(i) - \mathbf{p}0(i)}{\mathbf{p}_{\mathbf{upper}}(i) - \mathbf{p}_{\mathbf{lower}}(i)} \times N_{beta}$$

$$N_{beta} = 5 .$$

This sampling, weighted toward the original values, yielded a higher fraction of systems showing bistability. Sampling was repeated until we obtained 50 models that retained bistability with the ability to switch states when perturbed by species of the target list.

3.6.7 Relative robustness of dosing

For a pair of systems, one unperturbed system **p0** and one perturbed system **q**, and for a given pair of species (x1,x2), we study the relative robustness of the (x1,x2) dose combination to represent the relative change of combination doses versus non-combination doses. More formally, we define the relative robustness, RR, as follows:

$$\Delta CI = \sum_{i=1}^{2} \frac{rep\_xi\_q - rep\_xi\_p0}{critical\_xi\_q - critical\_xi\_p0} = \frac{\delta D1\_comb}{\delta D1} + \frac{\delta D2\_comb}{\delta D2}; \qquad (3)$$

$$RR = 1 - \Delta CI; \qquad (4)$$

where critical_xi_p0 denotes the critical dose of species xi from single species perturbation analysis in the model with original parameter setting; rep_xi_p0 denotes the xi component of representative dose combination in the model with original parameter setting; critical_xi_q denotes the critical dose of species xi from single species perturbation analysis in the model with perturbed parameters; rep_xi_q denotes the xi component of representative dose combination in the model with perturbed parameters. During single parameter perturbation analysis and multiple parameter perturbation analysis, we computed the RR for each perturbed model (compared with the original model), for each pair of species on the target list (Figure 3.3A-B, first row).

3.6.8 Correlation between synergism and robustness

For a pair of systems, perturbed and unperturbed, and for a given pair of species (x1,x2) we define the overall synergism to be the CI_{mid}:

$$CI_{mid} = (CI\_p0 + CI\_q)/2; \qquad (5)$$

where CI_p0 denotes the combination index of (x1,x2) in the model with original parameter setting using equation (2), and CI_q denotes the combination index of (x1,x2) in the model with perturbed parameters. We computed the CI_{mid} for each perturbed model (compared with the original model), for each pair of species on the target list (second row in Figure 3.3A-B). Finally, we compiled the mean RR for each pair of target species, across

all perturbed models, and the mean CI_{mid} across all perturbed models, for plotting in Figure 3.3C-D.

3.7 Conclusions

Through species perturbation and parameter perturbation analysis for a bistable TGF-β1 activation model, we found a correlation between synergism and relative robustness in combination therapy for bistable networks. Further analysis on multiple bistable models of various biological systems suggests that such correlation could be a general property of many bistable network models. The results of our study could be helpful in network modeling, drug discovery and the study of bistable biological decisions.

3.8 Supplementary Information

3.8.1 Supplementary figures

Figure 3.S1

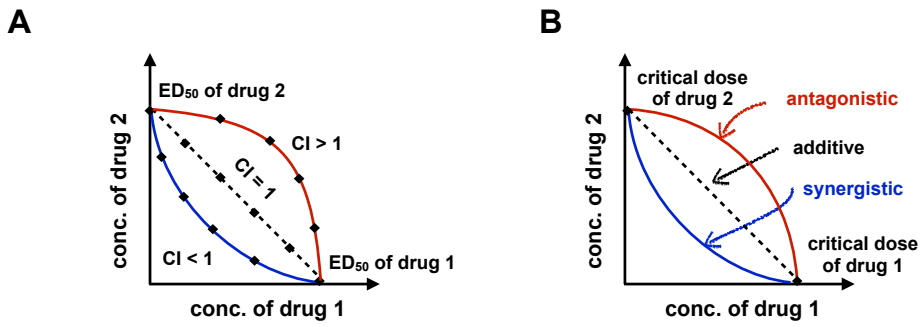

Figure 3.S1: Combination Index (CI) and its application in combination perturbation of bistale systems. The Combination Index (CI) and isobologram. (A) a classic ED50 isobologram for two drugs with actual doses on x- and y-axis. Dose combinations falling on the dotted line indicate

additive effect. Dose combinations falling on lower left (blue) indicate synergism. Dose combinations falling on upper right (red) indicate antagonism. (B) Separatrix in combination diagram of two drugs. Intercepts indicate the critical doses of the two drugs. Separatrix in a shape of straight line indicates additivity. Separatrix bending toward the origin (blue curve) indicates synergism. Separatrix in bending outward (red curve) indicate antagonism.

Figure 3.S2

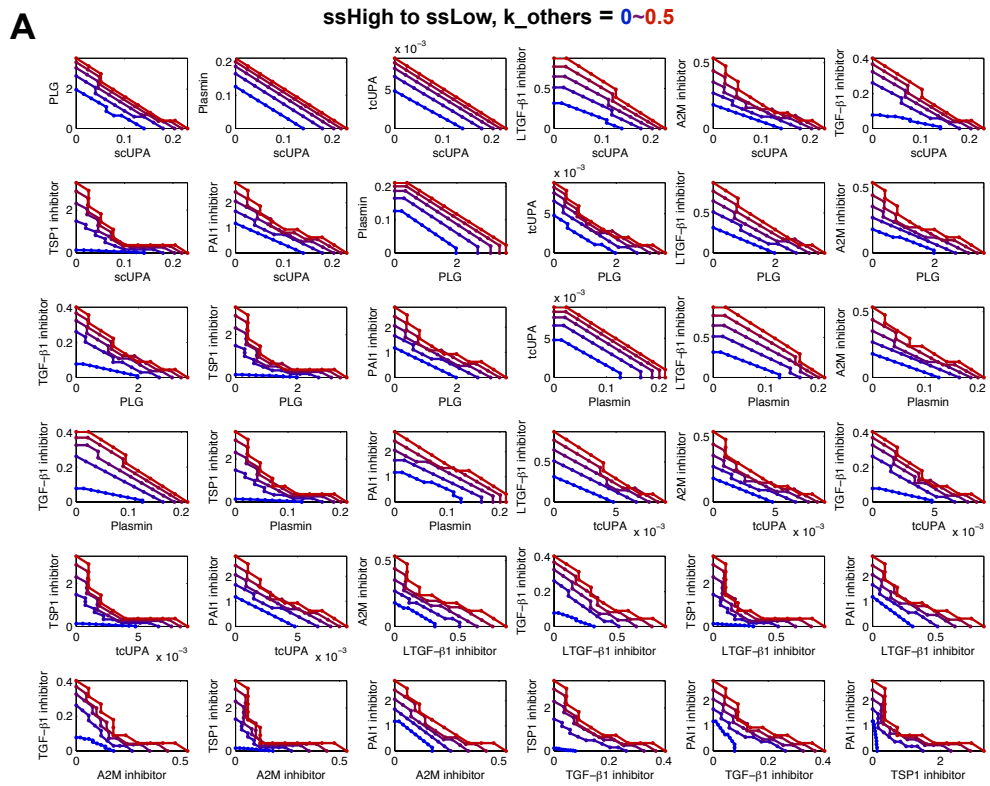
A
ssHigh to ssLow, k_others = 0~0.5
PLG
Plasmin
tcUPA
LTGF−β1 inhibitor
A2M inhibitor
TGF−β1 inhibitor
TSP1 inhibitor
PAI1 inhibitor
scUPA
PLG
Plasmin
tcUPA
LTGF−β1 inhibitor
A2M inhibitor

B

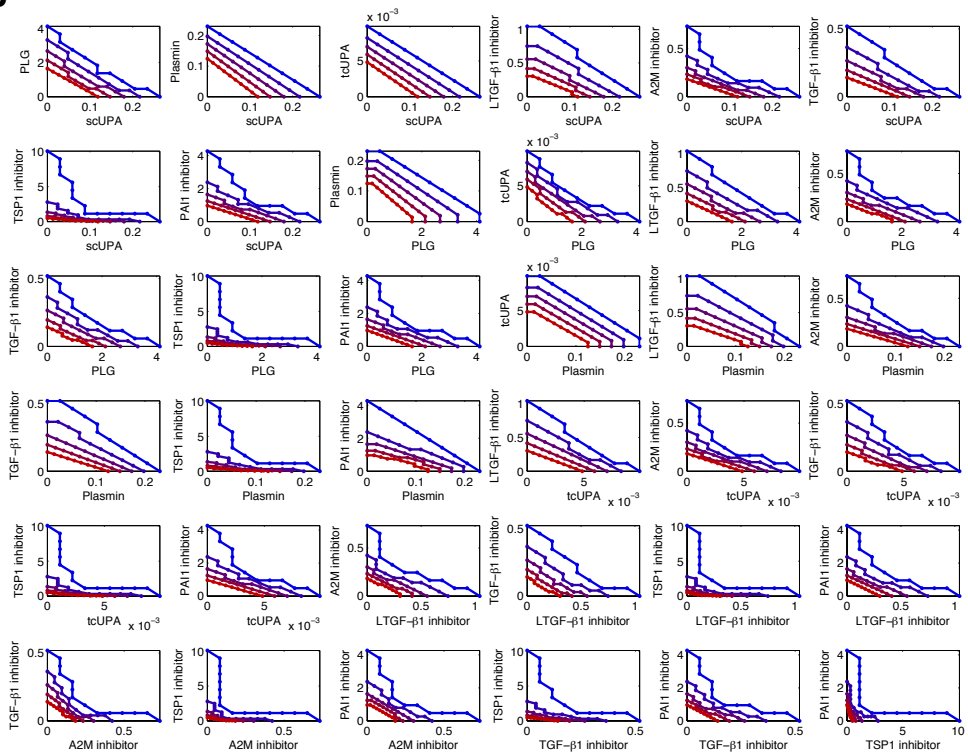
ssHigh to ssLow, keff2 = 0.26~0.61
PLG
Plasmin
tcUPA
LTGF−β1 inhibitor
A2M inhibitor
TGF−β1 inhibitor
TSP1 inhibitor
PAI1 inhibitor
scUPA
PLG
Plasmin
tcUPA
LTGF−β1 inhibitor
A2M inhibitor
TGF−β1 inhibitor
TSP1 inhibitor
PAI1 inhibitor
Plasmin
tcUPA
LTGF−β1 inhibitor
A2M inhibitor
TGF−β1 inhibitor
TSP1 inhibitor
PAI1 inhibitor
tcUPA
LTGF−β1 inhibitor
A2M inhibitor
TGF−β1 inhibitor
TSP1 inhibitor
PAI1 inhibitor
LTGF−β1 inhibitor
A2M inhibitor
TGF−β1 inhibitor
TSP1 inhibitor
PAI1 inhibitor
A2M inhibitor
TSP1 inhibitor
PAI1 inhibitor
TGF−β1 inhibitor

C

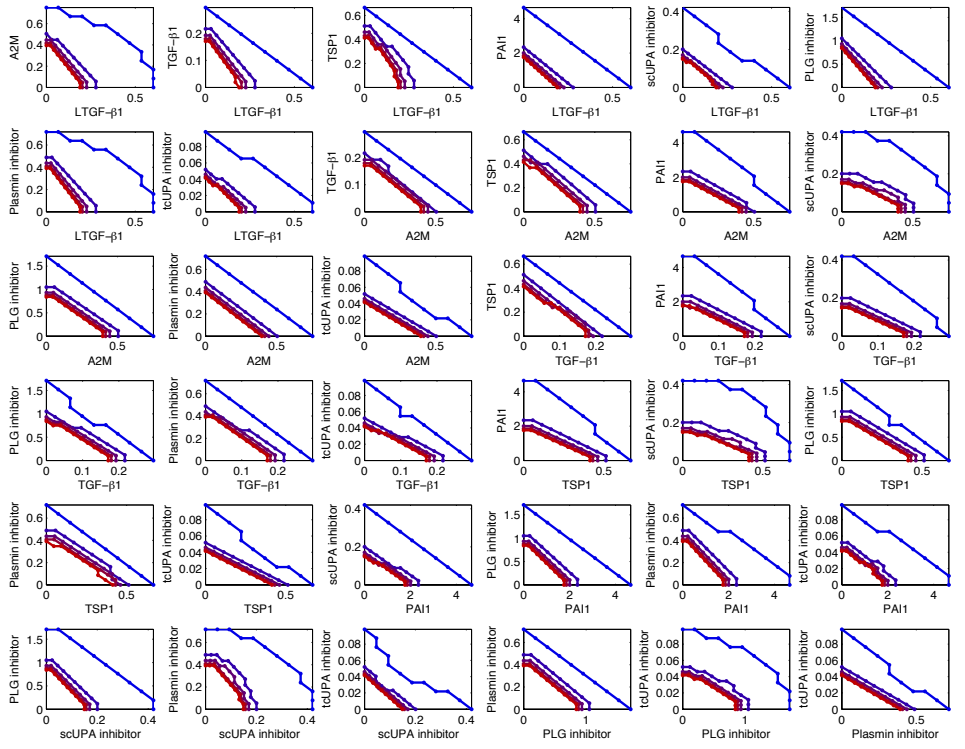
ssLow to ssHigh, k_others = 0~0.5
A2M
TGF−β1
TSP1
PAI1
scUPA inhibitor
PLG inhibitor
Plasmin inhibitor
tcUPA inhibitor
LTGF−β1
A2M
TGF−β1
PAI1
TSP1

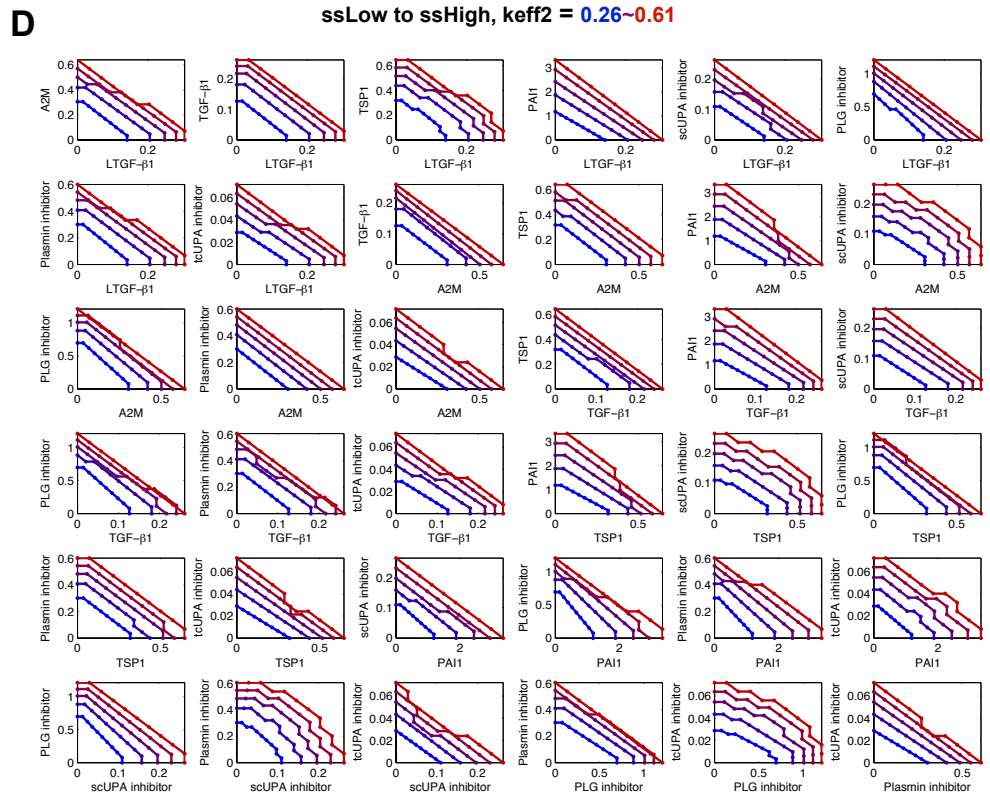

Figure 3.S2: Responses of all species combinations to parameter variation in the bistable TGF-β1 activation model. Responses of all species combination to different parameter variation in the bistable TGF-β1 activation model. (A) Shifts in the separatrix when the system changed its kothers value from 0 to 0.5 continuously. The bistable switch was from ssHigh to ssLow. (B) Shifts in the separatrix when the system changed its keff2 value from 0.26 to 0.61 continuously. The bistable switch was from ssHigh to ssLow. (C) Shifts in the separatrix when the system changed its kothers value from 0 to 0.5 continuously. The bistable switch was from ssLow to ssHigh. (D) Shifts in the separatrix when the system changed its keff2 value from 0.26 to 0.61 continuously. The bistable switch was from ssLow to ssHigh.

Figure 3.S3

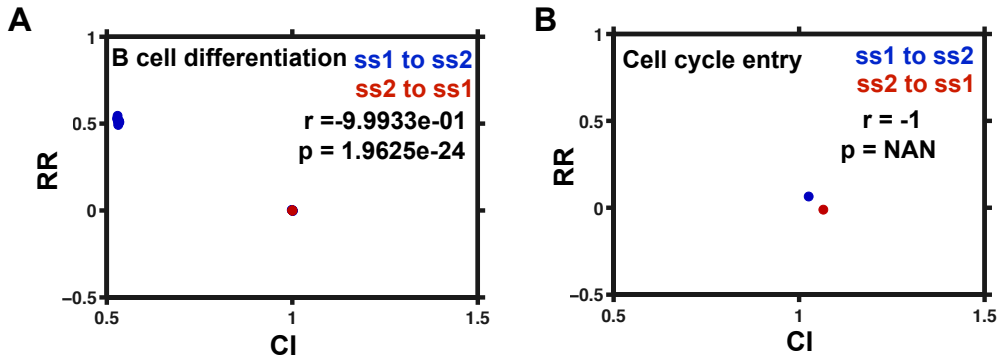

Figure 3.S3: Multiple parameter perturbation analysis of several other bistable models. In addition to Figure 3.4, several other models including (A) B cell differentiation model [88], and (B) cell cycle entry model were also tested with multiple parameter perturbation analysis [84]. The results suggested that their RR and CI_{mid} also follow the same pattern as models in Figure 3.3-4.

Figure 3.S4

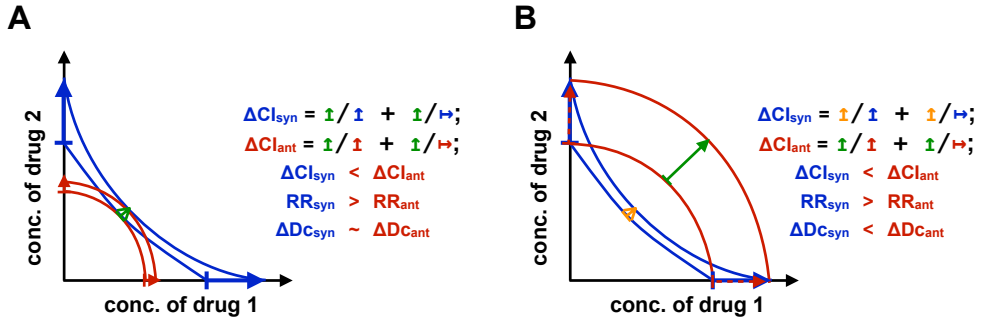

Figure 3.S4: Relative robustness (RR) and dose uncertainty. Diagrams of two typical cases of the dose variation of combination species perturbation. Synergistic combinations have smaller RR value compared with antagonistic combinations, but the actual dose uncertainty (or robustness) depends on the critical doses of their components, and the uncertainty (or robustness) of critical doses. (A) A synergistic combination and an antagonistic combination with similar combination dose uncertainty (or robustness). Blue curves represent the range of the combination critical doses (separatrix) of a synergistic combination. Blue arrows represent the uncertainty (variation) of the critical doses of its two components. Red curves represent the range of the combination critical doses (separatrix) of an antagonistic combination. Red

arrows represent the uncertainty (variation) of the critical doses of its two components. The green arrow represents the shared uncertainty (variation) of the representative critical dose combination (see Methods). Arrows were used in the equations to better reflect the qualitative difference in ΔCI and RR. The ratio between two arrows means the ratio between their x or y component. For example, ↥/↥ means the ratio between the y-components of green arrow and perpendicular blue arrow in the diagram, while ↥/↦ means the ratio between the x-components of green arrow and horizontal red arrow in the diagram. (B) A synergistic combination with better combination dose robustness than an antagonistic combination. Blue curves represent the range of the combination critical doses (separatrix) of a synergistic combination. Blue arrows represent the uncertainty (variation) of the critical doses of its two components. Red curves represent the range of the combination critical doses (separatrix) of an antagonistic combination. Red arrows represent the uncertainty (variation) of the critical doses of its two components. The green arrow represents the uncertainty (variation) of the representative critical dose combination of the antagonistic combination. The orange arrow represents the uncertainty (variation) of the representative critical dose combination of the synergistic combination (see Methods). Arrows were used in the equations to better reflect the qualitative difference in ΔCI and RR.

3.8.2 Supplementary tables

Table 3.S1: Bistable TGF-β1 activation model. (A) Steady state concentrations of species in TGF-β1 activation model. (B) Parameter values modeling the in inhibitors effects. (C) Critical doses of different species for two directions of bistable switch. (D) A list of combinations perturbations for two directions of bistable switch. Other details related with this model can be found in [1].

Table 3.S1A

species names	steady state concentrations	
	low TGF-β1 activation (μM)	high TGF-β1 activation (μM)
scUPA	0.0348	0.0179
PLG	1.8517	0.7032
LTGF-β1	0.0016	0.0087
A2M	0.1159	0.0008

species names	steady state concentrations	
Plasmin	0.0008	0.2736
tcUPA	0.0001	0.0226
TGF-β1	0.0153	0.0147
TSP1	0.0757	0.0010
PAI1	0.8205	0.8045

Table 3.S1B

parameter names	parameter values
k_inhibitors	20
deg_inhibitors	0.0175
deg_inhibitor_complexes	1
k_others	0.35

Table 3.S1C

anti TGF-β1 activation		pro TGF-β1 activation	
perturbation	critical dose	perturbation	critical dose
LTGF-β1 inhibition	0.7500	LTGF-β1 addition	0.2070
A2M inhibition	0.4219	A2M addition	0.4219
TGF-β1 inhibition	0.3672	TGF-β1 addition	0.1836
TSP1 inhibition	2.8125	TSP1 addition	0.4375
PAI1 inhibition	2.3750	PAI1 addition	1.8750
scUPA addition	0.2148	scUPA inhibition	0.1602
tcUPA addition	0.0083	tcUPA inhibition	0.0439
Plasmin addition	0.1992	Plasmin inhibition	0.4141

anti TGF-β1 activation		pro TGF-β1 activation	
PLG addition	3.3125	PLG inhibition	0.8906

Table 3.S1D

index	combination pairs	
	anti TGF-β1 activation	pro TGF-β1 activation
1	+scUPA and +PLG	+LTGF-β1 and +A2M
2	+scUPA and +Plasmi	+LTGF-β1 and +TGF-β1
3	+scUPA and +tcUPA	+LTGF-β1 and +TSP1
4	+scUPA and -LTGF-β	+LTGF-β1 and +PAI1
5	+scUPA and -A2M	+LTGF-β1 and -scUPA
6	+scUPA and -TGF-β1	+LTGF-β1 and -PLG
7	+scUPA and -TSP1	+LTGF-β1 and -Plasmin
8	+scUPA and -PAI1	+LTGF-β1 and -tcUPA
9	+PLG and +Plasmin	+A2M and +TGF-β1
10	+PLG and +tcUPA	+A2M and +TSP1
11	+PLG and -LTGF-β1	+A2M and +PAI1
12	+PLG and -A2M	+A2M and -scUPA
13	+PLG and -TGF-β1	+A2M and -PLG
14	+PLG and -TSP1	+A2M and -Plasmin
15	+PLG and -PAI1	+A2M and -tcUPA
16	+Plasmin and +tcUPA	+TGF-β1 and +TSP1
17	Plasmin and -LTGF-	+TGF-β1 and +PAI1
18	+Plasmin and -A2M	+TGF-β1 and -scUPA

index	combination pairs	
19	-Plasmin and -TGF-β	+TGF-β1 and -PLG
20	+Plasmin and -TSP1	+TGF-β1 and -Plasmin
21	+Plasmin and -PAI1	+TGF-β1 and -tcUPA
22	+tcUPA and -LTGF-β	+TSP1 and +PAI1
23	+tcUPA and -A2M	+TSP1 and -scUPA
24	+tcUPA and -TGF-β1	+TSP1 and -PLG
25	+tcUPA and -TSP1	+TSP1 and -Plasmin
26	+tcUPA and -PAI1	+TSP1 and -tcUPA
27	-LTGF-β1 and -A2M	+PAI1 and -scUPA
28	LTGF-β1 and -TGF-β	+PAI1 and -PLG
29	-LTGF-β1 and -TSP1	+PAI1 and -Plasmin
30	-LTGF-β1 and -PAI1	+PAI1 and -tcUPA
31	-A2M and -TGF-β1	-scUPA and -PLG
32	-A2M and -TSP1	-scUPA and -Plasmin
33	-A2M and -PAI1	-scUPA and -tcUPA
34	-TGF-β1 and -TSP1	-PLG and -Plasmin
35	-TGF-β1 and -PAI1	-PLG and -tcUPA
36	-TSP1 and -PAI1	-Plasmin and -tcUPA

Table 3.S2: Bistable Bcl2-apoptosis model. (A) Steady state concentrations of species. (B) Parameter values modeling the in inhibitors effects. (C) Critical doses of different species for two directions of bistable switch. (D) A list of combinations perturbations for two directions of bistable switch. Other details related with this model can be found in [85].

Table 3.S2A

species names	steady state concentrations	
	Non-apoptosis	apoptosis
InBax	39.6171	20.9680
AcBax	0.6758	5.3086

species names	steady state concentrations	
Bcl2	6.6641	1.2231
Act	0.7587	1.5996
ActBcl2	0.8426	0.3261
AcBaxBcl2	3.7531	5.4108
Ena	0.6429	0.9075
EnaBcl2	0.0714	0.0185
Mac	0.2657	1.3609

Table 3.S2B

parameter names	parameter values
k_inhibitors	1000
deg_inhibitors	0.01
deg_inhibitor_complexes	100
p2	0.020

Table 3.S2C

non-apoptotic to apoptotic		apoptotic to non-apoptotic	
perturbation	critical dose	perturbation	critical dose
InBax addition	26.5	InBax inhibition	8.625
AcBax addition	4.1875	AcBax inhibition	3.5
Bcl2 inhibition	5.125	Bcl2 addition	3.875
Act addition	5.5	Act inhibition	11
Ena addition	23	ActBcl2 addition	14.25
Mac addition	2.15625	EnaBcl2 addition	5.375
		Mac inhibition	1.84375

Table 3.S2D

index	combination pairs	
	non-apoptotic to apoptotic	apoptotic to non-apoptotic
1	+InBax and +AcBax	+Bcl2 and +ActBcl2
2	+InBax and +Act	+Bcl2 and +EnaBcl2
3	+InBax and +Ena	+Bcl2 and -InBax
4	+InBax and +Mac	+Bcl2 and -AcBax
5	+InBax and -Bcl2	+Bcl2 and -Act
6	+AcBax and +Act	+Bcl2 and -Mac
7	+AcBax and +Ena	+ActBcl2 and +EnaBcl2
8	+AcBax and +Mac	+ActBcl2 and -InBax
9	+AcBax and -Bcl2	+ActBcl2 and -AcBax
10	+Act and +Ena	+ActBcl2 and -Act
11	+Act and +Mac	+ActBcl2 and -Mac
12	+Act and -Bcl2	+EnaBcl2 and -InBax
13	+Ena and +Mac	+EnaBcl2 and -AcBax
14	+Ena and -Bcl2	+EnaBcl2 and -Act
15	+Mac and -Bcl2	+EnaBcl2 and -Mac
16		-InBax and -AcBax
17		-InBax and -Act
18		-InBax and -Mac
19		-AcBax and -Act
20		-AcBax and -Mac
21		-Act and -Mac

Table 3.S3: Bistable hematopeietic cell fate model. (A) Steady state concentrations of species. (B) Parameter values modeling the in inhibitors effects. (C) Critical doses of different species for two directions of bistable switch. (D) A list of combinations perturbations for two directions of bistable switch. Other details related with this model can be found in [89].

Table 3.S3A

species names	steady state concentrations	
	s.s. Neut	s.s. Mac
M1	0.0161	2.0000
N1	2.0000	2.0000
M2	0.0006	3.3333
N2	3.3333	0.0268
M3	0.0003	3.8769
N3	3.1081	0.0073

Table 3.S3B

parameter names	parameter values
k_inhibitors	10
deg_inhibitors	0.01
deg_inhibitor_complexes	10
eM	2
eN	2
nA	1
nR	4
alpha	5
alpha_lo	1
alpha_hi	4

Table 3.S3C

s.s. Neut to s.s. Mac		s.s. Mac to s.s. Neut	
perturbation	critical dose	perturbation	critical dose
N1 inhibition	6.5	M1 inhibition	5.25

s.s. Neut to s.s. Mac		s.s. Mac to s.s. Neut	
M2 addition	5.25	M2 inhibition	3.5
N2 inhibition	4.6875	N2 addition	2.8125

Table 3.S3D

index	combination pairs	
	s.s. Neut to s.s. Mac	s.s. Mac to s.s. Neut
1	+M2 and -N1	+N2 and -M1
2	+M2 and -N2	+N2 and -M2
3	-N1 and -N2	-M1 and -M2

Table 3.S4: A top-robust ETT bistable motif model. (A) Steady state concentrations of species. (B) Parameter values modeling the in inhibitors effects. (C) Critical doses of different species for two directions of bistable switch. (D) A list of combinations perturbations for two directions of bistable switch. Other details related with this model can be found in [99].

Table 3.S4A

species names	steady state concentrations	
	s.s. 1	s.s. 2
A	0.0127	0.0004
As	0.0035	0.0002
B	38.7106	1.3194
Bs	31.1522	0.0071
C	39.5378	1.6391
Cs	96.9751	0.0073
AsB	1.5100	0.0032
AsC	1.5423	0.0040

Table 3.S4B

parameter names	parameter values
k_inhibitors	1000
deg_inhibitors	0.01
deg_inhibitor_complexes	100
k0	954.4394
k1	56.9482
k2	27.8277
kP	107.7107
kQ	431.3992
Ksyn	1.5481
KP	0.0112
KQ	0.2579
v	0.6996
bsyn	0.0100
kdeg	0.0100
P	0.0100
Q	0.1000
S	0.1292

Table 3.S4C

s.s. 1 to s.s. 2		s.s. 2 to s.s. 1	
perturbation	critical dose	perturbation	critical dose
A inhibition	12.2105102539062	As addition	5639.71875
As inhibition	3.28744506835938	B addition	292.369140625
B inhibition	1606.6640625	Bs addition	131.83935546875
Bs inhibition	1333.421875	C addition	284.171875
C inhibition	86.0712890625	Cs addition	125.69140625
Cs inhibition	113.3955078125		

Table 3.S4D

index	combination pairs	
	s.s. 1 to s.s. 2	s.s. 1 to s.s. 2
1	-A and -As	+As and +B
2	-A and -B	+As and +Bs
3	-A and -Bs	+As and +C
4	-A and -C	+As and +Cs
5	-A and -Cs	+B and +Bs
6	-As and -B	+B and +C
7	-As and -Bs	+B and +Cs
8	-As and -C	+Bs and +C
9	-As and -Cs	+Bs and +Cs
10	-B and -Bs	+C and +Cs
11	-B and -C	
12	-B and -Cs	
13	-Bs and -C	
14	-Bs and -Cs	
15	-C and -Cs	

Table 3.S5: B-cell differentiation model. (A) Steady state concentrations of species. (B) Parameter values modeling the in inhibitors effects. (C) Critical doses of different species for two directions of bistable switch. (D) A list of combinations perturbations for two directions of bistable switch. Other details related with this model can be found in [88].

Table 3.S5A

species names	steady state concentrations	
	s.s. Blimp1 high	s.s. Blimp1 low
Bcl6_gene1	0.0205	1.7972
Bcl6_mRNA	0.0369	3.2312
Bcl6	2.1296	186.5584
Blimp1_gene1	1.0288	0.0011
Blimp1_mRNA	1.8497	0.0020
Blimp1	106.7945	0.1129

species names	steady state concentrations	
Pax5_gene1	0.0054	1.2296
Pax5_mRNA	0.0096	2.2106
Pax5	0.5560	127.6340
AP1p	77.0246	77.0246
TA	1554.5499	1554.5499
TAA	1345.4007	1345.4007

Table 3.S5B

parameter names	parameter values
k_inhibitors	1000
deg_inhibitors	0.01
deg_inhibitor_complexes	100
LPS	0.2
TCDD	0.5

Table 3.S5C

s.s. Blimp1 high to s.s. Blimp1 low		s.s. Blimp1 low to s.s. Blimp1 high	
perturbation	critical dose	perturbation	critical dose
Bcl6_gene1 addition	2816	Blimp1_gene 1 addition	1408
Bcl6_mRNA addition	61	Blimp1_mR NA addition	5.125
Bcl6 addition	3200	Blimp1 addition	272
Pax5_gene1 addition	1280		
Pax5_mRN A addition	7.125		
Pax5 addition	376		

Table 3.S5D

index	combination pairs	
	s.s. Blimp1 high to s.s. Blimp1 low	s.s. Blimp1 low to s.s. Blimp1 high
1	cl6_gene1 and +Bcl6_mR	+Blimp1_gene1 and +Blimp1_mRNA
2	+Bcl6_gene1 and +Bcl6	+Blimp1_gene1 and +Blimp1
3	cl6_gene1 and +Pax5_ge	+Blimp1_mRNA and +Blimp1
4	cl6_gene1 and +Pax5_mRNA	
5	+Bcl6_gene1 and +Pax5	
6	+Bcl6_mRNA and +Bcl6	
7	cl6_mRNA and +Pax5_gene1	
8	l6_mRNA and +Pax5_mRNA	
9	+Bcl6_mRNA and +Pax5	
10	+Bcl6 and +Pax5_gene1	
11	+Bcl6 and +Pax5_mRNA	
12	+Bcl6 and +Pax5	
13	ax5_gene1 and +Pax5_mRNA	
14	+Pax5_gene1 and +Pax5	
15	+Pax5_mRNA and +Pax5	

Table 3.S6: Bistable cell cycle entry model. (A) Steady state concentrations of species. (B) Parameter values modeling the in inhibitors effects. (C) Critical doses of different species for two directions of bistable switch. (D) A list of combinations perturbations for two directions of bistable switch. Other details related with this model can be found in [84].

Table 3.S6A

species names	steady state concentrations	
	s.s. “on”	s.s. “off”
MD	0.9989	0.0000
RP	0.0000	1.0000
EE	1.9685	0.0000

Table 3.S6B

parameter names	parameter values
k_inhibitors	1000
deg_inhibitors	0.01
deg_inhibitor_complexes	100
S	0.0100
tMD	1.0000
tRP	1.0000
tEE	1.0000
n1	5.0000
k1	0.5000
n2	5.0000
k2	0.5000
n3	5.0000
k3	0.5000
n5	5.0000
k5	0.5000
n6	5.0000
k6	0.5000
n7	5.0000
k7	0.5000
n9	5.0000
k9	0.5000
tMD	1.0000
tEE	1.0000

Table 3.S6C

s.s. “on” to s.s. “off”		s.s. “off” to s.s. “on”	
perturbation	critical dose	perturbation	critical dose
RP addition	3.5625	MD addition	1.9375
EE inhibition	2.125	EE addition	0.96875

Table 3.S6D

index	combination pairs	
	s.s. “on” to s.s. “off”	s.s. “off” to s.s. “on”
1	+RP and -EE	+MD and +EE

CHAPTER 4: CONCLUSIONS

Rational design of anti-TGF-β1 therapies depends upon systems level understanding of TGF-β1 regulation in liver fibrosis. Recently the systems biology approach has been introduced to study TGF-β1 regulation in liver fibrosis [1,2]. Computational modeling and simulation has been shown to be a great approach to reveal systems level dynamics in various biological systems. Following this approach, we have identified the effects of two factors on the TGF-β1 bistability, and how one of them can affect the sign of feedback loops within the network. We have also identified properties of inducing a bistable switch via combination perturbation for the TGF-β1 bistable activation model, and shown similar properties in models of many other bistable biological systems. Our work has extended the current understanding of TGF-β1 bistable activation on systems level, built up computational methods to study combination therapy on bistable biological systems, and revealed several correlation relationships between different properties of the same network.

In our first work, we used computational modeling to explore the implications of a bistable TGF-β1 activation network, and we found (a) upstream factors like calcium and KLF2 could affect the steady state behavior of this bistable system, and (b) the steady state behavior of the system correlates with the sign of a feedback loop in the network. For the first part, we modeled known effects of calcium on the balance between TSP1 and PLS [33,35,51-54], and known effects of KLF2 on the gene expression of PAI1 and TSP1 [37]. We

then used modeling to show how these effects would propagate through the system. Specifically, the model predicted that calcium would significantly promote TGF-β1 activation, shifting the bistable threshold of the system. The calcium-induced increase in TSP1 would lie within the physiological range of TSP1 [55]. In contrast, KLF2 was simulated to increase PLS activity and decrease the levels of TGF-β1, by suppressing PAI1 and TSP1 expression. This is consistent with previous work with statin drugs on liver fibrosis [36], where KLF2 upregulation was observed after treatment with simvastatin. Our model predicts that one of the ways KLF2 may contribute to improvement of liver fibrosis may be by decreasing the activation of TGF-β1 through reduction of the TSP1 and PAI feedback effects. While modeling KLF2 effects, we noticed that loss of bistability also caused a change in the sign of the PLS - PAI1 feedback loop. There is some support in the published literature that the relationship between PLS and PAI can show either negative feedback or positive feedback, depending on context [48-50]. In our model, we found that without KLF2, the PLS-PAI1 feedback loop was positive (double negative), but with KLF2 (100% KLF2) and with the destruction of bistability, the PLS-PAI1 feedback loop was negative. Additional bifurcation analysis revealed that high KLF2 is a special case of the general observation, that the bistability of the system is correlated with the sign of the PLS-PAI1 feedback loop. An *in vitro* experiment validated the positive feedback behavior between PLS and PAI1 in a bistable TGF-β1 system.

In our second work, we studied the problem of combination targeting of bistable systems with our bistable TGF-β1 activation system. We found that different target combinations yielded different levels of synergism. More interestingly, we found that the synergism of a combination was related to the robustness. To be precise, when model parameters underwent modest fluctuations (within the bistable regime of the system), the relative robustness of the combination doses was positively correlated with the combination index. The parameter fluctuations were performed by applying single-parameter and multiple-parameter perturbation methods. The relative robustness was defined by the sum of relative changes of combination doses over single doses as defined by equations (3)-(4) in section **3.6.7**, and the synergy was defined by the combination index (CI) method. After repeating the same analysis on several other bistable network models, all cases exhibited some degree of positive correlation between RR (relative robustness) and synergy (negative correlation between RR and CI). This suggests that a correlation between robustness and synergism may be a general property of combination dosing for many bistable network models. Robustness analysis has been used to deal with uncertainty in network modeling. This traditional use of robustness analysis is complemented by our use of robustness analysis to study **dose robustness.** Our discovery that the relative robustness of critical combination doses is negatively correlated with Combination Index (CI) (positively correlated with synergy) provides a prediction that administering a synergistic combination of treatments can be a choice to increase the dose

robustness of the treatment. Synergistic treatments are by definition able to achieve the same efficacy with lower doses (compared with non-synergistic combinations), and here we show that they also have the potential to achieve a narrower confidence interval on the therapeutic effect, in the presence of uncertainty.

There are several caveats that should temper the interpretation of our modeling results. Firstly, the model used kinetics rate constants that were not known experimentally. Thus the behavior of the model should be taken as a qualitative prediction of trends rather than a quantitative prediction of absolute magnitude. Secondly, parameters taken from previous publications may be incorrect for our context, even if they were correct for the original context in which they were published. Thirdly, we have simplified complex processes into simplistic scalar variables. For example, even the effect of calcium on TSP1 has been greatly simplified, relative to the true effect, which is a change in the equilibrium between different conformations of TSP1. The simplified nature of our model implies that its predictions are low-resolution trends, not detailed molecular concentrations. Fourthly, although the correlation relationships between qualitative properties have already considered the model uncertainty to some extent, and some of them are quite solid, experimental validation are still required to test the validity of the model and its behavior.

By connecting information from different biological sources, we showed that computational models can guide us to hypothesize systems-level regulatory mechanisms. Model predictions of this sort, whether or not the predictions are

quantitatively accurate, may be useful for elucidating the network level vocabulary of TGF-β1 regulatory mechanisms that can effect systems-level coordination. We anticipate that these predicted hypotheses will help accelerate future experimental studies.

To sum up, through the analysis of network dynamics, we have broadened our current understanding of TGF-β1 regulation in liver fibrosis on a system level. When studying the TGF-β1 bistable system, we have identified important implications for bistable systems, and combination therapy. The focus of future work should include experimental validation of the predictions that have been made, and looking for correlation relationships between properties of TGF-β1 bitable systems, other bistable biological systems, biological systems in general using a computational and systems biology approach.

CHAPTER 5: FUTURE DIRECTIONS

5.1 Transient Dynamics and Non-monotonic Behaviors During Bistable Switch

5.1.1 Motivation

The bistable model of TGF-β1 activation implies bistable behavior not just for itself but also for the species along its feedback loops (PAI1, urokinase plasmin activator (uPA), PLS, and TSP1), not to mention effects on other proteins outside the scope of the model. Furthermore, in addition to steady-state behaviors and feedback loops, transient effects may also be modeled, meaning system behaviors prior to steady-state convergence. The implications of these aspects have not yet been studied, and would be important for understanding the functions of these proteins in various disease contexts.

5.1.2 The transition towards the low TGF-β1 steady state causes transient angiogenic effects

We are particularly interested in system behavior during a switch transition from ssT to ssP. For example, a variety of anti-TGF-β therapeutics has entered clinical trials [110], and might cause the TGF-β1 activation system to switch states. Even in the absence of drugs, the subsystem of PLS activation is bistable [90], and healthy regulation of clotting might involve sharp increases in PLS levels. If sharp changes do occur in PLS activity, how would they affect the transient behavior of the TGF-β1 network? Transient behavior

could have important effects on vasculature, where TSP1 and PLS are master-regulators of angiogenesis and coagulation. During simulations of a transition from ssT to ssP, we noticed a variety of transient effects that could be significant for angiogenesis. TSP1 has multiple mechanisms for opposing angiogenesis [111-114], while PLS has multiple proangiogenic effects [115,116], in addition to cleaving TSP1. After TSP1 is cleaved, its N-terminal domain has strong pro-angiogenic effects [117-119], indicative of a matrikine effect with short half-life (fast degradation rate) [120,121].

Reaction number	Reaction equation	Reaction number	Reaction equation
1	$scUPA + PLG \xrightarrow{keff_1} PLS + scUPA$	12,13	$A2M + PLS \underset{k_{-5}}{\overset{k_5}{\rightleftarrows}} A2M:PLS$
2	$PLS + scUPA \xrightarrow{keff_2} tcUPA + PLS$	14,15	$PAI1 + tcUPA \underset{k_{-6}}{\overset{k_6}{\rightleftarrows}} PAI1:tcUPA$
3	$tcUPA + PLG \xrightarrow{keff_3} PLS + tcUPA$	16,17	$PAI1 + scUPA \underset{k7}{\overset{k_7}{\rightleftarrows}} PAI1:scUPA$
4	$PLS + LTGF\beta1 \xrightarrow{k_1} TGF\beta1 + PLS$	18	$PLS + scUPA \xrightarrow{keff_2} tcUPA + PLS$
5	$TSP1 + LTGF\beta1 \xrightarrow{k_2} TGF\beta1 + PLS$	19	$PLS + scUPA \xrightarrow{keff_2} tcUPA + PLS$
6	$LTGF\beta1 \xrightarrow{k_{others}} TGF\beta1$	20	$TSP1:PLS \xrightarrow{k_8}$
7	$TGF\beta1 \xrightarrow{kp_1} TSP1$	21	$TGF\beta1 \xrightarrow{k_9}$
8	$TGF\beta1 \xrightarrow{kp_2} PAI1$	production	$\xrightarrow{\alpha_1}\{scUPA;\ LTGF\beta1;\ A2M\};\ \xrightarrow{\alpha_2}\{PLG\}$
9,10	$TSP1 + PLS \underset{k_{-3}}{\overset{k_3}{\rightleftarrows}} TSP1:PLS$	degradation	$\{scUPA;\ LTGF\beta1;\ A2M\} \xrightarrow{\mu_{edeg}}$; {all other protein species} $\xrightarrow{\mu_{pdeg}}$
11	$TSP1:PLS \xrightarrow{k_4} PLS + cleaved\_TSP1$	degradation (b)	$\{cleaved\_TSP1\} \xrightarrow{\mu_{cTSP1\_deg}}$

Table 5.1: List of equations and parameters used for model construction

We created a new species "cleaved_TSP1" to represent the angiogenic fragments yielded from one molecule of TSP1 in the "angiogenesis model". The cleaved_TSP1 species was inserted into equation 11 (Table 5.1). Finally, cleaved_TSP1 was assigned a fast degradation rate ($1s^{-1}$). We calculated the "integrated angiogenic signal" from the levels of PLS, TSP1, and cleaved_TSP1 using the following formula:

$$\text{AngioSignal} = w_{\text{PLS}} \times \text{PLS} + w_{\text{TSP1}} \times \text{TSP1} + w_{\text{cleaved\_TSP1}} \times \text{cleaved\_TSP1},$$

where

$w_{\text{PLS}} = 0.01,$

$w_{\text{TSP1}} = 0.1,$

$w_{\text{cleaved\_TSP1}} = 1000.$

Starting with the model in the ssT state (TGF-β1 high steady state), we perturbed individual species and tracked how these perturbations would affect the net angiogenic signal, both transiently and after convergence to one of the steady states. Figure 5.1A shows that a sufficient dose of PLS could switch the system from ssT (with angiogenesis suppressed) into ssP with increased angiogenesis. Because the angiogenic signal is defined by including PLS as a pro-angiogenic factor, any increase in PLS necessarily caused an instantaneous increase in the angiogenic signal (comparing the angiogenic signal immediately before and after the addition). Quite interestingly, a perturbation to increase PLS also caused a second, later wave of transient side-effects, including a spike in the angio- genic signal, before converging to a steady state (Figure 5.1A). This shows that, the bistable model of TGF-β1 is capable of producing non-monotonic concentrations during a switch, and some species can exhibit extreme levels during the transition.

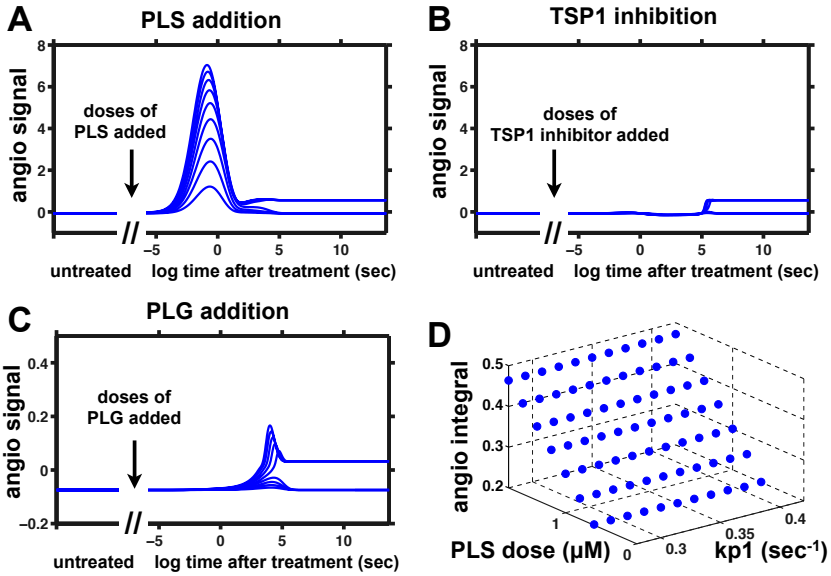

Figure 5.1: PLG/Plasmin have strong angiogenic effect. (A) angiogenic signal of PLS addition into low TGF-β1 activation steady state, with degradation rate of cleaved TSP1 being 1 s^{-1}. (B) angiogenic signal of TSP1 inhibition into low TGF-β1 activation steady state, with degradation rate of cleaved TSP1 being 1 s^{-1}. (C) angiogenic signal of PLG addition into low TGF-β1 activation steady state, with degradation rate of cleaved TSP1 being 100 s^{-1}. (D) dependence of PLS addition angiogenic signal on PLS dose, with degradation rate of cleaved TSP1 being 1 s^{-1}. In this figure, the simulation is done with low calcium condition, and [KLF2] = 0%.

Not all transitions from ssT to ssP induced a spike in the angiogenic signal. For example, inhibiting TSP1 can switch the system, but during a TSP1-induced switch, the transient level of angiogenic signaling was moderate and the direction of change was nearly monotonic (Figure 5.1B).

Finally we calculated the dependence of the angiogenic signal on the PLG and PLS dose, and on the parameters of the model. Figure 5.1C shows that the

timing of the angiogenic spike is sensitive to the reaction rates in the model, which were unknown. This case, with an alternative set of parameters, achieved a long-lasting spike of the angiogenic effect (a peak until 10^5s is roughly one day) after simulation with PLG. Next we calculated the integrated angiogenic signal, which we defined as the integral of the angio- genic signal time-course, minus the ssP level of angiogenic signal. In figure 5.1D, the integrated angiogenic signal was linearly correlated with the dose of PLS, but was relatively insensitive to the rate parameters, for parameter changes ± 20%. Figure 5.1D shows an example of this for the rate parameter kp1, which is the rate of TSP1 production. In sum, our model consistently predicts a transient angiogenic effect, but the nature of the prediction is qualitative, not quantitative.

We do not know how often a "TGF-β1 high" (ssT) tissue would transit towards a "TGF-β1 low" (ssP) state *in vivo*. Successful wound healing is an orderly progression of distinct phases, and in such well-reguglated cases, the transition away from a TGF-β1 high state might occur infrequently [122-124]. Pathologically excessive wound healing, such as fibrosis, may have dramatic swings with both abnormally high and abnormally low levels of PLS or coagulation proteins [125-127]. Liver fibrosis is characterized by pathological blood flow, including abundant sprouting of vessels [128,129], with poor delivery of oxygen and nutrients [130]. In other words, fibrosis has too many partially-formed blood vessels, and too much initiation of angiogenesis, but not enough complete, functional blood vessels. Future work should examine

whether pulses of pro-angiogenic influence, such as shown in Figure 5.1 contribute to the disruption of vessel formation and to the pathological angiogenesis seen in fibrotic tissues.

5.1.3 Non-monotonic behavior during bistable switch

The pulse-like influence towards angiogenesis we have found could be a special case of some general property of bistable systems. The essence of our insight is that the species concentrations in a bistable system do not necessarily progress monotonically from one steady state to the other. In the TGF-β1 bistable model, the fibrosis-like ssT state enforces low levels of PLS levels by preventing the activation of PLG (the inactive precursor of PLS). PLG has a relatively long half-life, so it accumulates to a high level in the ssT state. During a switch transition from ssT to ssP, this vast reservoir of PLG is converted suddenly into PLS, causing PLS levels to spike even higher than the ssP level. This is true regardless of angiogenic side-effects. For example, Figure 5.2 shows that exogenous addition of PLS caused a second later spike in the PLS level, because positive feedback converted the reservoir of latent PLG into PLS. Another non-monotonic effect occurs with the level of cleaved TSP1. The ssT levels of TSP1 are high, again like a reservoir of TSP1. During the ssT to ssP transition, the sudden spike in PLS causes sudden cleavage of TSP1 into cleaved_TSP1. The spike in cleaved_TSP1 causes a large fold-change in the overall angiogenic effect [117-119].

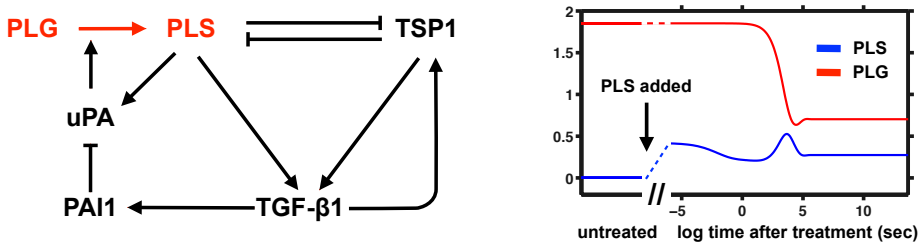

Figure 5.2: Nonmonotonic effect during bistable transition in a TGF-β1 activation network

Future work should examine the co-existence of "reservoir" molecules and the non-monotonic behavior of their "active" forms in other network models. Systems with non-monotonic behavior allow small perturbations to induce a much stronger innate response, therefore a better understanding of non-monotonic behavior in general would be valuable for the problem of drug target selection in the future.

5.2 In Vitro Study of Anti-TGF-β1 Combination Therapy

Many anti-TGF-β1 strategies have shown effects in animal models of liver fibrosis [16]. These strategies include modifications of TGF-β1 receptor , using antibodies against TGF-β1, blockage of TGF-β1 activation, and over expression of Smad7. Blockage of TGF-β1 activation is an important type of strategy targeting the process of latent-TGF-β1 (LTGF-β1) activation. Previous studies have shown the effect of targeting the plasmin-activation pathway and the TSP1 activation pathway individually. For the plasmin

activation pathway, in vivo overexpression of UPA or knockout of PAI1 caused a decrease in the level of TGF-β1 and fibrosis [23,24]. For the TSP1 activation pathway, a peptide Leu-Ser-Lys-Leu (LSKL) that can inhibit TSP1-dependent latent TGF-β1 activation prevented the progression of liver fibrosis in DMN rats [21]. Despite the remarkable progress of anti-TGF-β1 therapies, the research on combination therapy for liver fibrosis is still in its early phase. A study has indicated that the combination delivery of uPA and HGF could confer synergistic anti-fibrotic effect [131]. However, due to the lack of systems level understanding of TGF-β1 regulation during liver fibrosis, the choice of combination targets was mainly made empirically.

Systems biology and network modeling enables systems level design and in silico screening of combination targets. In Chapter 3, computational simulation has shown the combination effects of different target combinations. Future work should check whether such differences in synergy can be observed experimentally. The hepatocyte-HSC co-culture model described in Chapter 2 can serve as the in vitro experimental system. In vitro hits can then be tested on animal models.

BIBLIOGRAPHY

1. Venkatraman L, Chia S-M, Narmada BC, White JK, Bhowmick SS, et al. (2012) Plasmin Triggers a Switch-Like Decrease in Thrombospondin-Dependent Activation of TGF-β1. Biophys J 103: 1060–1068. doi:10.1016/j.bpj.2012.06.050.

2. Narmada BC, Chia S-M, Tucker-Kellogg L, Yu H (2012) HGF regulates the activation of TGF-β1 in rat hepatocytes and hepatic stellate cells. J Cell Physiol 228: 393–401. doi:10.1002/jcp.24143.

3. Kitano H (2002) Systems Biology: A Brief Overview. Science 295: 1662–1664. doi:10.1126/science.1069492.

4. Aldridge BB, Burke JM, Lauffenburger DA, Sorger PK (2006) Physicochemical modelling of cell signalling pathways. Nat Cell Biol 8: 1195–1203. doi:10.1038/ncb1497.

5. Sobie EA (2011) Bistability in Biochemical Signaling Models. Sci Signal 4: tr10. doi:10.1126/scisignal.2001964.

6. Ingalls BP (2013) Mathematical Modeling in Systems Biology: An Introduction. 1st ed. The MIT Press. p.

7. Kholodenko BN, Demin OV, Moehren G, Hoek JB (1999) Quantification of short term signaling by the epidermal growth factor receptor. J Biol Chem 274: 30169–30181.

8. Sasagawa S, Ozaki Y-I, Fujita K, Kuroda S (2005) Prediction and validation of the distinct dynamics of transient and sustained ERK activation. Nat Cell Biol 7: 365–373. doi:10.1038/ncb1233.

9. Park CS, Schneider IC, Haugh JM (2003) Kinetic analysis of platelet-derived growth factor receptor/phosphoinositide 3-kinase/Akt signaling in fibroblasts. J Biol Chem 278: 37064–37072. doi:10.1074/jbc.M304968200.

10. Kogan Y, Halevi-Tobias KE, Hochman G, Baczmanska AK, Leyns L, et al. (2012) A new validated mathematical model of the Wnt signalling pathway predicts effective combinational therapy by sFRP and Dkk.

Biochem J 444: 115–125. doi:10.1042/BJ20111887.

11. Hornberg JJ, Binder B, Bruggeman FJ, Schoeberl B, Heinrich R, et al. (2005) Control of MAPK signalling: from complexity to what really matters. Oncogene 24: 5533–5542. doi:10.1038/sj.onc.1208817.

12. Fitzgerald JB, Schoeberl B, Nielsen UB, Sorger PK (2006) Systems biology and combination therapy in the quest for clinical efficacy. Nature Chemical Biology 2: 458–466. doi:10.1038/nchembio817.

13. Bataller R, Brenner DA (2005) Liver fibrosis. J Clin Invest 115: 209–218. doi:10.1172/JCI24282.

14. Friedman S (2008) Hepatic stellate cells: protean, multifunctional, and enigmatic cells of the liver. Physiol Rev.

15. Gressner A, Weiskirchen R, Breitkopf K, Dooley S (2002) Roles of TGF-beta in hepatic fibrosis. Front Biosci.

16. Breitkopf K, Haas S, Wiercinska E (2006) Anti-TGF-β Strategies for the Treatment of Chronic Liver Disease - Breitkopf - 2006 - Alcoholism: Clinical and Experimental Research - Wiley Online Library. Alcoholism: Clinical ….

17. Cheng K, Yang N, Mahato RI (2009) TGF-beta1 gene silencing for treating liver fibrosis. Mol Pharm 6: 772–779. doi:10.1021/mp9000469.

18. Annes JP, Munger JS, Rifkin DB (2003) Making sense of latent TGFbeta activation. J Cell Sci 116: 217–224.

19. Murphy-Ullrich JE, Poczatek M (2000) Activation of latent TGF-beta by thrombospondin-1: mechanisms and physiology. Cytokine Growth Factor Rev 11: 59–69.

20. Crawford SE, Stellmach V, Murphy-Ullrich JE, Ribeiro SM, Lawler J, et al. (1998) Thrombospondin-1 is a major activator of TGF-beta1 in vivo. Cell 93: 1159–1170.

21. Kondou H, Mushiake S, Etani Y, Miyoshi Y, Michigami T, et al. (2003) A blocking peptide for transforming growth factor-beta1 activation prevents hepatic fibrosis in vivo. J Hepatol 39: 742–748.

22. Lyons RM, Gentry LE, Purchio AF, Moses HL (1990) Mechanism of activation of latent recombinant transforming growth factor beta 1 by plasmin. J Cell Biol 110: 1361–1367.

23. Martínez-Rizo A, Bueno-Topete M, González-Cuevas J, Armendáriz-Borunda J (2010) Plasmin plays a key role in the regulation of profibrogenic molecules in hepatic stellate cells. Liver Int 30: 298–310. doi:10.1111/j.1478-3231.2009.02155.x.

24. Huang Y, Haraguchi M, Lawrence DA, Border WA, Yu L, et al. (2003) A mutant, noninhibitory plasminogen activator inhibitor type 1 decreases matrix accumulation in experimental glomerulonephritis. J Clin Invest 112: 379–388. doi:10.1172/JCI18038.

25. Inoue H, Yokoyama F, Kita Y, Yoshiji H, Tsujimoto T, et al. (2006) Relationship between the proliferative capability of hepatocytes and the intrahepatic expression of hepatocyte growth factor and c-Met in the course of cirrhosis development in rats. Int J Mol Med 17: 857–864.

26. Li F, Sun J-Y, Wang J-Y, Du S-L, Lu W-Y, et al. (2008) Effect of hepatocyte growth factor encapsulated in targeted liposomes on liver cirrhosis. J Control Release 131: 77–82. doi:10.1016/j.jconrel. 2008.07.021.

27. Horiguchi K, Hirano T, Ueki T, Hirakawa K, Fujimoto J (2009) Treating liver cirrhosis in dogs with hepatocyte growth factor gene therapy via the hepatic artery. J Hepatobiliary Pancreat Surg 16: 171–177. doi: 10.1007/s00534-008-0029-7.

28. Kutz SM, Hordines J, McKeown-Longo PJ, Higgins PJ (2001) TGF-beta1-induced PAI-1 gene expression requires MEK activity and cell-to-substrate adhesion. J Cell Sci 114: 3905–3914.

29. Thorsen S, Philips M, Selmer J, Lecander I, Astedt B (1988) Kinetics of inhibition of tissue-type and urokinase-type plasminogen activator by plasminogen-activator inhibitor type 1 and type 2. Eur J Biochem 175: 33–39.

30. Sajid M, Lele M, Stouffer GA (2000) Autocrine thrombospondin partially mediates TGF-beta1- induced proliferation of vascular smooth

muscle cells. Am J Physiol Heart Circ Physiol 279: H2159–H2165.

31. Mimura Y, Ihn H, Jinnin M, Asano Y, Yamane K, et al. (2005) Constitutive thrombospondin-1 overexpression contributes to autocrine transforming growth factor-beta signaling in cultured scleroderma fibroblasts. Am J Pathol 166: 1451–1463.

32. Bonnefoy A, Legrand C (2000) Proteolysis of subendothelial adhesive glycoproteins (fibronectin, thrombospondin, and von Willebrand factor) by plasmin, leukocyte cathepsin G, and elastase. Thromb Res 98: 323–332.

33. Hogg PJ, Stenflo J, Mosher DF (1992) Thrombospondin is a slow tight-binding inhibitor of plasmin. Biochemistry 31: 265–269.

34. Anonick PK, Yoo JK, Webb DJ, Gonias SL (1993) Characterization of the antiplasmin activity of human thrombospondin-1 in solution. Biochem J 289 (Pt 3): 903–909.

35. Gotis-Graham I, Hogg PJ, McNeil HP (1997) Significant correlation between thrombospondin 1 and serine proteinase expression in rheumatoid synovium. Arthritis Rheum 40: 1780–1787. doi: 10.1002/1529-0131(199710)40:10<1780::AID-ART9>3.0.CO;2-L.

36. Marrone G, Russo L, Rosado E, Hide D, García-Cardeña G, et al. (2012) The transcription factor KLF2 mediates hepatic endothelial protection and paracrine endothelial-stellate cell deactivation induced by statins. J Hepatol. doi:10.1016/j.jhep.2012.08.026.

37. Dekker RJ (2006) KLF2 provokes a gene expression pattern that establishes functional quiescent differentiation of the endothelium. Blood 107: 4354–4363. doi:10.1182/blood-2005-08-3465.

38. Boon RA, Fledderus JO, Volger OL, van Wanrooij EJA, Pardali E, et al. (2007) KLF2 suppresses TGF-beta signaling in endothelium through induction of Smad7 and inhibition of AP-1. Arterioscler Thromb Vasc Biol 27: 532–539. doi:10.1161/01.ATV.0000256466.65450.ce.

39. Strogatz SH (2008) Nonlinear Dynamics and Chaos. Westview Press. p.

40. Neves S, Iyengar R (2002) Modeling of signaling networks - Neves -

2002 - BioEssays - Wiley Online Library. Bioessays.

41. Ratushny AV, Saleem RA, Sitko K, Ramsey SA, Aitchison JD (2012) Asymmetric positive feedback loops reliably control biological responses. Mol Syst Biol 8: 577. doi:10.1038/msb.2012.10.

42. Tsai TY-C, Choi YS, Ma W, Pomerening JR, Tang C, et al. (2008) Robust, tunable biological oscillations from interlinked positive and negative feedback loops. Science 321: 126–129. doi:10.1126/science.1156951.

43. Grainger DJ, Wakefield L, Bethell HW, Farndale RW, Metcalfe JC (1995) Release and activation of platelet latent TGF-beta in blood clots during dissolution with plasmin. Nature Medicine 1: 932–937. Available:http://eutils.ncbi.nlm.nih.gov/entrez/eutils/elink.fcgi?dbfrom=pubmed&id=7585220&retmode=ref&cmd=prlinks.

44. Khalil N, Corne S, Whitman C, Yacyshyn H (1996) Plasmin regulates the activation of cell-associated latent TGF-beta 1 secreted by rat alveolar macrophages after in vivo bleomycin injury. Am J Respir Cell Mol Biol 15: 252–259.

45. Yee JA, Yan L, Dominguez JC, Allan EH, Martin TJ (1993) Plasminogen-dependent activation of latent transforming growth factor beta (TGF beta) by growing cultures of osteoblast-like cells. J Cell Physiol 157: 528–534. doi:10.1002/jcp.1041570312.

46. Godár S, Horejsi V, Weidle UH, Binder BR, Hansmann C, et al. (1999) M6P/IGFII-receptor complexes urokinase receptor and plasminogen for activation of transforming growth factor-beta1. Eur J Immunol 29: 1004–1013. doi:10.1002/(SICI)1521-4141(199903)29:03<1004::AID-IMMU1004>3.0.CO;2-Q.

47. Binder BR, Christ G, Gruber F, Grubic N, Hufnagl P, et al. (2002) Plasminogen activator inhibitor 1: physiological and pathophysiological roles. News Physiol Sci 17: 56–61.

48. Thornton AJ, Bruzdzinski CJ, Raper SE, Gelehrter TD (1994) Plasminogen activator inhibitor-1 is an immediate early response gene in

regenerating rat liver. Cancer Res 54: 1337–1343.

49. Flaumenhaft R, Abe M, Mignatti P, Rifkin DB (1992) Basic fibroblast growth factor-induced activation of latent transforming growth factor beta in endothelial cells: regulation of plasminogen activator activity. J Cell Biol 118: 901–909.

50. Seo JY, Park J, Yu MR, Kim YS, Ha H, et al. (2009) Positive Feedback Loop between Plasminogen Activator Inhibitor-1 and Transforming Growth Factor-Beta1 during Renal Fibrosis in Diabetes. Am J Nephrol 30: 481–490. doi:10.1159/000242477.

51. Calzada MJ, Kuznetsova SA, Sipes JM, Rodrigues RG, Cashel JA, et al. (2008) Calcium indirectly regulates immunochemical reactivity and functional activities of the N-domain of thrombospondin-1. Matrix Biol 27: 339–351. doi:10.1016/j.matbio.2007.12.002.

52. Dixit VM, Galvin NJ, O'Rourke KM, Frazier WA (1986) Monoclonal antibodies that recognize calcium-dependent structures of human thrombospondin. Characterization and mapping of their epitopes. J Biol Chem 261: 1962–1968.

53. Misenheimer TM, Mosher DF (1995) Calcium ion binding to thrombospondin 1. J Biol Chem 270: 1729–1733.

54. Slane JM, Mosher DF, Lai CS (1988) Conformational change in thrombospondin induced by removal of bound Ca2+. A spin label approach. FEBS Lett 229: 363–366.

55. Bergseth G, Lappegård KT, Videm V, Mollnes TE (2000) A novel enzyme immunoassay for plasma thrombospondin. Comparison with beta-thromboglobulin as platelet activation marker in vitro and in vivo. Thromb Res 99: 41–50.

56. Branton MH, Kopp JB (1999) ScienceDirect.com - Microbes and Infection - TGF-β and fibrosis. Microbes Infect 1: 1349–1365.

57. Wang H, Zhang Y, Heuckeroth RO (2007) PAI-1 deficiency reduces liver fibrosis after bile duct ligation in mice through activation of tPA. FEBS Lett 581: 3098–3104. doi:10.1016/j.febslet.2007.05.049.

58. Hugo C (2003) The thrombospondin 1-TGF-beta axis in fibrotic renal disease. Nephrol Dial Transplant 18: 1241–1245.

59. Mazzieri R, Munger JS, Rifkin DB (2000) Measurement of active TGF-beta generated by cultured cells. Methods Mol Biol 142: 13–27. doi: 10.1385/1-59259-053-5:13.

60. Erbas H, Erten O, Irfanoglu ME (2008) Breast cyst fluid plasmin activity and its effect on TGF-beta2 activation. Cancer Invest 26: 22–27. doi: 10.1080/07357900701638004.

61. Bourd-Boittin K, Bonnier D, Leyme A, Mari B, Tuffery P, et al. (2011) Protease profiling of liver fibrosis reveals the ADAM metallopeptidase with thrombospondin type 1 motif, 1 as a central activator of transforming growth factor beta. Hepatology 54: 2173–2184. doi: 10.1002/hep.24598.

62. Sato Y, Rifkin DB (1989) Inhibition of endothelial cell movement by pericytes and smooth muscle cells: activation of a latent transforming growth factor-beta 1-like molecule by plasmin during co-culture. J Cell Biol 109: 309–315.

63. Yu Q, Stamenkovic I (2000) Cell surface-localized matrix metalloproteinase-9 proteolytically activates TGF-beta and promotes tumor invasion and angiogenesis. Genes Dev 14: 163–176.

64. Prudova A, auf dem Keller U, Butler GS, Overall CM (2010) Multiplex N-terminome analysis of MMP-2 and MMP-9 substrate degradomes by iTRAQ-TAILS quantitative proteomics. Mol Cell Proteomics 9: 894–911. doi:10.1074/mcp.M000050-MCP201.

65. Lawler PR, Lawler J (2012) Molecular basis for the regulation of angiogenesis by thrombospondin-1 and -2. Cold Spring Harb Perspect Med 2: a006627. doi:10.1101/cshperspect.a006627.

66. Hogg PJ, Owensby DA, Mosher DF, Misenheimer TM, Chesterman CN (1993) Thrombospondin is a tight-binding competitive inhibitor of neutrophil elastase. J Biol Chem 268: 7139–7146.

67. Bein K, Simons M (2000) Thrombospondin type 1 repeats interact with

matrix metalloproteinase 2. Regulation of metalloproteinase activity. J Biol Chem 275: 32167–32173. doi:10.1074/jbc.M003834200.

68. Davis GE, Pintar Allen KA, Salazar R, Maxwell SA (2001) Matrix metalloproteinase-1 and -9 activation by plasmin regulates a novel endothelial cell-mediated mechanism of collagen gel contraction and capillary tube regression in three-dimensional collagen matrices. J Cell Sci 114: 917–930.

69. Curry TE, Osteen KG (2003) The matrix metalloproteinase system: changes, regulation, and impact throughout the ovarian and uterine reproductive cycle. Endocr Rev 24: 428–465.

70. Annes JP, Chen Y, Munger JS, Rifkin DB (2004) Integrin alphaVbeta6-mediated activation of latent TGF-beta requires the latent TGF-beta binding protein-1. J Cell Biol 165: 723–734. doi:10.1083/jcb.200312172.

71. Kaartinen V, Warburton D (2003) Fibrillin controls TGF-beta activation. Nat Genet 33: 331–332. doi:10.1038/ng0303-331.

72. Tritschler I, Gramatzki D, Capper D, Mittelbronn M, Meyermann R, et al. (2009) Modulation of TGF-beta activity by latent TGF-beta-binding protein 1 in human malignant glioma cells. Int J Cancer 125: 530–540. doi:10.1002/ijc.24443.

73. Chaudhry SS, Cain SA, Morgan A, Dallas SL, Shuttleworth CA, et al. (2007) Fibrillin-1 regulates the bioavailability of TGFbeta1. J Cell Biol 176: 355–367. doi:10.1083/jcb.200608167.

74. Buscemi L, Ramonet D, Klingberg F, Formey A, Smith-Clerc J, et al. (2011) The single-molecule mechanics of the latent TGF-β1 complex. Curr Biol 21: 2046–2054. doi:10.1016/j.cub.2011.11.037.

75. Ahamed J, Janczak CA, Wittkowski KM, Coller BS (2009) PLOS ONE: In Vitro and In Vivo Evidence that Thrombospondin-1 (TSP-1) Contributes to Stirring- and Shear-Dependent Activation of Platelet-Derived TGF-β1. PLoS ONE 4: e6608. doi:10.1371/journal.pone.0006608.t001.

76. Kirschner R, Hubmacher D, Iyengar G, Kaur J, Fagotto-Kaufmann C, et al. (2011) Classical and neonatal Marfan syndrome mutations in fibrillin-1 cause differential protease susceptibilities and protein function. J Biol Chem 286: 32810–32823. doi:10.1074/jbc.M111.221804.

77. Fontana L, Chen Y, Prijatelj P, Sakai T, Fässler R, et al. (2005) Fibronectin is required for integrin alphavbeta6-mediated activation of latent TGF-beta complexes containing LTBP-1. FASEB J 19: 1798–1808. doi:10.1096/fj.05-4134com.

78. Toettcher JE, Apgar JF, Castillo AR, Tidor B, White J (2011) Simulation and Verification of Electronic and Biological Systems. Li P, Silveira LM, Feldmann P, editors Dordrecht: Springer Netherlands. pp. doi: 10.1007/978-94-007-0149-6_6.

79. Seglen PO (1976) Preparation of isolated rat liver cells. Methods Cell Biol 13: 29–83.

80. Chatterjee A, Kaznessis YN, Hu W-S (2008) Tweaking biological switches through a better understanding of bistability behavior. Current Opinion in Biotechnology 19: 475–481. doi:10.1016/j.copbio.2008.08.010.

81. Tian T, Burrage K (2006) Stochastic models for regulatory networks of the genetic toggle switch. Proc Natl Acad Sci USA 103: 8372–8377. doi: 10.1073/pnas.0507818103.

82. Frigola D, Casanellas L, Sancho JM, Ibañes M (2012) Asymmetric stochastic switching driven by intrinsic molecular noise. PLoS ONE 7: e31407. doi:10.1371/journal.pone.0031407.

83. Albeck JG, Burke JM, Spencer SL, Lauffenburger DA, Sorger PK (2008) Modeling a snap-action, variable-delay switch controlling extrinsic cell death. PLoS Biol 6: 2831–2852. doi:10.1371/journal.pbio.0060299.

84. Yao G, Tan C, West M, Nevins JR, You L (2011) Origin of bistability underlying mammalian cell cycle entry. Mol Syst Biol 7: 485. doi: 10.1038/msb.2011.19.

85. Cui J, Chen C, Lu H, Sun T, Shen P (2008) Two independent positive feedbacks and bistability in the Bcl-2 apoptotic switch. PLoS ONE 3: e1469. doi:10.1371/journal.pone.0001469.

86. Bagci EZ, Vodovotz Y, Billiar TR, Ermentrout GB, Bahar I (2006) Bistability in apoptosis: roles of bax, bcl-2, and mitochondrial permeability transition pores. Biophys J 90: 1546–1559. doi:10.1529/biophysj.105.068122.

87. Shi Y, Mellier G, Huang S, White J, Pervaiz S, et al. (2013) Computational modelling of LY303511 and TRAIL-induced apoptosis suggests dynamic regulation of cFLIP. Bioinformatics 29: 347–354. doi:10.1093/bioinformatics/bts702.

88. Bhattacharya S, Conolly RB, Kaminski NE, Thomas RS, Andersen ME, et al. (2010) A Bistable Switch Underlying B-Cell Differentiation and Its Disruption by the Environmental Contaminant 2,3,7,8-Tetrachlorodibenzo-p-dioxin.

89. Laslo P, Spooner CJ, Warmflash A, Lancki DW, Lee H-J, et al. (2006) Multilineage transcriptional priming and determination of alternate hematopoietic cell fates. Cell 126: 755–766. doi:10.1016/j.cell.2006.06.052.

90. Venkatraman L, Li H, Dewey CF, White JK, Bhowmick SS, et al. (2011) Steady states and dynamics of urokinase-mediated plasmin activation in silico and in vitro. Biophys J 101: 1825–1834. doi:10.1016/j.bpj.2011.08.054.

91. Craciun G, Tang Y, Feinberg M (2006) Understanding bistability in complex enzyme-driven reaction networks. Proc Natl Acad Sci USA 103: 8697–8702. doi:10.1073/pnas.0602767103.

92. Gardner TS, Cantor CR, Collins JJ (2000) Construction of a genetic toggle switch in Escherichia coli. Nature 403: 339–342. doi:10.1038/35002131.

93. Csermely P, Agoston V, Pongor S (2005) The efficiency of multi-target drugs: the network approach might help drug design. Trends Pharmacol Sci 26: 178–182. doi:10.1016/j.tips.2005.02.007.

94. Agoston V, Csermely P, Pongor S (2005) Multiple weak hits confuse complex systems: a transcriptional regulatory network as an example. Phys Rev E Stat Nonlin Soft Matter Phys 71: 051909.

95. Araujo RP, Petricoin EF, Liotta LA (2005) A mathematical model of combination therapy using the EGFR signaling network. BioSystems 80: 57–69. doi:10.1016/j.biosystems.2004.10.002.

96. Chou T-C, Talalay P (1984) Quantitative analysis of dose-effect relationships: the combined effects of multiple drugs or enzyme inhibitors. Advances in Enzyme Regulation 22: 27–55. doi: 10.1016/0065-2571(84)90007-4.

97. Huang L, Pan CQ, Li B, Tucker-Kellogg L, Tidor B, et al. (2011) Simulating EGFR-ERK signaling control by scaffold proteins KSR and MP1 reveals differential ligand-sensitivity co-regulated by Cbl-CIN85 and endophilin. PLoS ONE 6: e22933. doi:10.1371/journal.pone. 0022933.

98. Chua HE, Bhowmick SS, Tucker-Kellogg L, Dewey CF Jr. (2012) Proceedings of the ACM Conference on Bioinformatics, Computational Biology and Biomedicine - BCB '12. in silico heuristic target combination identification for disease-related signaling networks. New York, New York, USA: ACM Press. pp. 4–11. doi: 10.1145/2382936.2382937.

99. Shah NA, Sarkar CA (2011) Robust network topologies for generating switch-like cellular responses. PLoS Comput Biol 7: e1002085. doi: 10.1371/journal.pcbi.1002085.

100. Chou T-C (2006) Theoretical basis, experimental design, and computerized simulation of synergism and antagonism in drug combination studies. Pharmacol Rev 58: 621–681. doi:10.1124/pr. 58.3.10.

101. Nim TH, Luo L, Clement MV, White JK, Tucker-Kellogg L (2013) Systematic parameter estimation in data-rich environments for cell signalling dynamics. Bioinformatics 29: 1044–1051. doi:10.1093/ bioinformatics/btt083.

102. Kim J, Bates DG, Postlethwaite I, Ma L, Iglesias PA (2006) Robustness analysis of biochemical network models. Syst Biol (Stevenage) 153: 96–104.

103. Kitano H (2007) A robustness-based approach to systems-oriented drug design. Nat Rev Drug Discov 6: 202–210. doi:10.1038/nrd2195.

104. Perumal T, Wu Y, Gunawan R (2008) Robustness Analysis of Cellular Systems for In Silico Drug Discovery. 17th World Congress-The International ….

105. Nayak S, Salim S, Luan D, Zai M, Varner J (2008) A test of highly optimized tolerance reveals fragile cell-cycle mechanisms are molecular targets in clinical cancer trials. PLoS ONE.

106. Eissing T, Allgöwer F, Bullinger E (2005) Robustness properties of apoptosis models with respect to parameter variations and intrinsic noise. Syst Biol (Stevenage) 152: 221–228.

107. Mahdavi A, Davey RE, Bhola P, Yin T, Zandstra PW (2007) Sensitivity analysis of intracellular signaling pathway kinetics predicts targets for stem cell fate control. PLoS Comput Biol 3: e130. doi:10.1371/journal.pcbi.0030130.

108. Luan D, Zai M, Varner JD (2007) Computationally derived points of fragility of a human cascade are consistent with current therapeutic strategies. PLoS Comput Biol 3: e142. doi:10.1371/journal.pcbi.0030142.

109. Guidelines for industry: Dose-response information to support drug registration. (n.d.) Guidelines for industry: Dose-response information to support drug registration.

110. Calone I, Souchelnytskyi S (2012) Inhibition of TGFβ signaling and its implications in anticancer treatments. Exp Oncol 34: 9–16.

111. Garside SA, Harlow CR, Hillier SG, Fraser HM, Thomas FH (2010) Thrombospondin-1 inhibits angiogenesis and promotes follicular atresia in a novel in vitro angiogenesis assay. Endocrinology 151: 1280–1289. doi:10.1210/en.2009-0686.

112. Sheibani N, Newman PJ, Frazier WA (1997) Thrombospondin-1, a natural inhibitor of angiogenesis, regulates platelet-endothelial cell adhesion molecule-1 expression and endothelial cell morphogenesis. Mol Biol Cell 8: 1329–1341.

113. Bornstein P (2009) Thrombospondins function as regulators of angiogenesis. J Cell Commun Signal 3: 189–200. doi:10.1007/s12079-009-0060-8.

114. Zak S, Treven J, Nash N, Gutierrez LS (2008) Lack of thrombospondin-1 increases angiogenesis in a model of chronic inflammatory bowel disease. Int J Colorectal Dis 23: 297–304. doi:10.1007/s00384-007-0397-5.

115. Rakic JM, Maillard C, Jost M, Bajou K, Masson V, et al. (2003) Role of plasminogen activator-plasmin system in tumor angiogenesis. Cell Mol Life Sci 60: 463–473.

116. Oh C, Plow JH, Plow E (2003) The role of plasminogen in angiogenesis in vivo - Oh - 2003 - Journal of Thrombosis and Haemostasis - Wiley Online Library. Journal of Thrombosis and ….

117. Morandi V (2009) The N-terminal domain of thrombospondin-1: a key for the dual effect of TSP-1 in angiogenesis and cancer progression? ScientificWorldJournal 9: 133–136. doi:10.1100/tsw.2009.11.

118. Dias JV, Benslimane-Ahmim Z, Egot M, Lokajczyk A, Grelac F, et al. (2012) A motif within the N-terminal domain of TSP-1 specifically promotes the proangiogenic activity of endothelial colony-forming cells. Biochemical Pharmacology 84: 1014–1023. doi:10.1016/j.bcp.2012.07.006.

119. Ann Elzie C, Murphy-Ullrich JE (2004) The N-terminus of thrombospondin: the domain stands apart. The International Journal of Biochemistry & Cell Biology 36: 1090–1101. doi:10.1016/j.biocel.2003.12.012.

120. Burgess JK, Weckmann M (2012) Matrikines and the lungs. Pharmacol Ther 134: 317–337. doi:10.1016/j.pharmthera.2012.02.002.

121. Rosca EV, Koskimaki JE, Rivera CG, Pandey NB, Tamiz AP, et al. (2011) Anti-angiogenic peptides for cancer therapeutics. Curr Pharm Biotechnol 12: 1101–1116.

122. Liu W, Wang D, Cao Y (2004) TGF-b: A Fibrotic Factor in Wound Scarring and a Potential Target for Anti- Scarring Gene Therapy. CGT 4: 123–136. doi:10.2174/1566523044578004.

123. Amento EP, Beck LS (1991) TGF-beta and wound healing. Ciba Found Symp 157: 115–23–discussion123–9.

124. Wang X-J, Han G, Owens P, Siddiqui Y, Li AG (2006) Role of TGF beta-mediated inflammation in cutaneous wound healing. J Investig Dermatol Symp Proc 11: 112–117.

125. Northup PG (2009) Hypercoagulation in liver disease. Clin Liver Dis 13: 109–116. doi:10.1016/j.cld.2008.09.003.

126. Calvaruso V, Maimone S, Gatt A, Tuddenham E, Thursz M, et al. (2008) Coagulation and fibrosis in chronic liver disease. Gut 57: 1722–1727. doi:10.1136/gut.2008.150748.

127. Lisman T, Leebeek FWG (2007) Hemostatic alterations in liver disease: a review on pathophysiology, clinical consequences, and treatment. Dig Surg 24: 250–258. doi:10.1159/000103655.

128. Thabut D, Shah V (2010) Intrahepatic angiogenesis and sinusoidal remodeling in chronic liver disease: new targets for the treatment of portal hypertension? J Hepatol 53: 976–980. doi:10.1016/j.jhep. 2010.07.004.

129. Fernández M, Semela D, Bruix J, Colle I, Pinzani M, et al. (2009) Angiogenesis in liver disease. J Hepatol 50: 604–620. doi:10.1016/ j.jhep.2008.12.011.

130. Paternostro C, David E, Novo E, Parola M (2010) Hypoxia, angiogenesis and liver fibrogenesis in the progression of chronic liver diseases. World J Gastroenterol 16: 281–288.

131. Lin Y, Xie W-F, Chen Y-X, Zhang X, Zeng X, et al. (2005) Treatment of experimental hepatic fibrosis by combinational delivery of urokinase-

type plasminogen activator and hepatocyte growth factor genes. Liver Int 25: 796–807. doi:10.1111/j.1478-3231.2005.01098.x.